nature medicine

TCF1 links GIPR signaling to the control of beta cell function and survival

Jonathan E Campbell[1], John R Ussher[1,7], Erin E Mulvihill[1], Jelena Kolic[2,3], Laurie L Baggio[1], Xiemen Cao[1], Yu Liu[1], Benjamin J Lamont[1,7], Tsukasa Morii[1,7], Catherine J Streutker[4], Natalia Tamarina[5], Louis H Philipson[5], Jeffrey L Wrana[1], Patrick E MacDonald[2,3] & Daniel J Drucker[1,6]

The glucagon-like peptide-1 (GLP-1) receptor and the glucose-dependent insulinotropic polypeptide (GIP) receptor transduce nutrient-stimulated signals to control beta cell function[1]. Although the GLP-1 receptor (GLP-1R) is a validated drug target for diabetes[1], the importance of the GIP receptor (GIPR) for the function of beta cells remains uncertain[2–4]. We demonstrate that mice with selective ablation of GIPR in beta cells (*MIP-Cre:Gipr*$^{Flox/Flox}$*; Gipr*$^{-/-\beta Cell}$) exhibit lower levels of meal-stimulated insulin secretion, decreased expansion of adipose tissue mass and preservation of insulin sensitivity when compared to *MIP-Cre* controls. Beta cells from *Gipr*$^{-/-\beta Cell}$ mice display greater sensitivity to apoptosis and markedly lower islet expression of T cell–specific transcription factor-1 (TCF1, encoded by *Tcf7*), a protein not previously characterized in beta cells. GIP, but not GLP-1, promotes beta cell *Tcf7* expression via a cyclic adenosine monophosphate (cAMP)-independent and extracellular signal–regulated kinase (ERK)-dependent pathway. *Tcf7* (in mice) or *TCF7* (in humans) levels are lower in islets taken from diabetic mice and in humans with type 2 diabetes; knockdown of *TCF7* in human and mouse islets impairs the cytoprotective responsiveness to GIP and enhances the magnitude of apoptotic injury, whereas restoring TCF1 levels in beta cells from *Gipr*$^{-/-\beta Cell}$ mice lowers the number of apoptotic cells compared to that seen in *MIP-Cre* controls. *Tcf7*$^{-/-}$ mice show impaired insulin secretion, deterioration of glucose tolerance with either aging and/or high-fat feeding and increased sensitivity to beta cell injury relative to wild-type (WT) controls. Hence the GIPR-TCF1 axis represents a potential therapeutic target for preserving both the function and survival of vulnerable, diabetic beta cells.

The ingestion of nutrients triggers the secretion of multiple gut peptides, including GLP-1 and GIP, both of which are incretin hormones that amplify insulin secretion. GLP-1 and GIP also control beta cell growth and survival[1], rendering them attractive targets for the treatment of type 2 diabetes (T2D). Indeed, the prevention of incretin degradation by inhibiting dipeptidyl peptidase-4 (DPP4)[5] and the augmentation of incretin receptor signaling using GLP-1R agonists or emerging co- and tri-agonists that target this pathway[6,7] represent established and investigational strategies for the treatment of T2D.

The receptors for GLP-1 and GIP are highly related in structure; both are regulated by transcription factor 7-like 2 (TCF7L2)[8] in islets and control beta cell function and survival through cAMP-dependent pathways. Although genetic variation within the coding region of the *GLP1R* gene has been linked to differences in fasting glucose levels and in beta cell function in humans[9], interpretation of the importance of the GIPR for beta cell function is confounded by genetic and physiological data in humans and in mice and rats that suggest roles for the GIPR in the regulation of adipose-tissue accretion, body weight and insulin sensitivity[2–4,10].

GLP-1R agonists are increasingly used for the treatment of T2D and obesity and are under investigation for the treatment of type 1 diabetes[1,11]. By contrast, there is less interest in the GIPR as a drug target because of reports of defective GIP action in people with diabetes who are severely hyperglycemic[12]. Nevertheless, a brief period of insulin therapy markedly restores GIP responsiveness in subjects with T2D (ref. 13), and GIPR activation is a key component of the action of several novel co- and tri-agonists that are under investigation as potential treatments for diabetes and obesity[6,7]. Accordingly, to delineate the importance of GIPR signaling in beta cells independently of its potentially confounding actions in extrapancreatic tissues, we mated *MIP-Cre*ERT mice with *Gipr*$^{Flox/Flox}$ mice to generate mice with conditional and selective inactivation of *Gipr* in adult beta cells (*Gipr*$^{-/-\beta Cell}$) (**Supplementary Fig. 1a**). Levels of *Gipr* mRNA transcripts were 90% lower in the islets of *Gipr*$^{-/-\beta Cell}$ mice than in those of *MIP-Cre* mice, *Gipr*$^{Flox/Flox}$ mice and WT mice (**Fig. 1a** and **Supplementary Fig. 1b**), whereas *Gipr* expression in adipose tissue was not perturbed (**Supplementary Fig. 1b**). GIP robustly reduced

[1]Lunenfeld-Tanenbaum Research Institute, Mt. Sinai Hospital, Toronto, Ontario, Canada. [2]Department of Pharmacology, University of Alberta, Edmonton, Alberta, Canada. [3]Alberta Diabetes Institute, University of Alberta, Edmonton, Alberta, Canada. [4]St. Michael's Hospital, University of Toronto, Toronto, Ontario, Canada. [5]Department of Medicine, Kovler Diabetes Center, University of Chicago, Chicago, USA. [6]Department of Medicine, University of Toronto, Toronto, Ontario, Canada. [7]Present addresses: Faculty of Pharmacy and Pharmaceutical Sciences, University of Alberta, Edmonton, Alberta, Canada (J.R.U.); Department of Medicine, University of Melbourne, Melbourne, Australia (B.J.L.); Akita University Graduate School of Medicine, Akita, Japan (T.M.). Correspondence should be addressed to D.J.D. (drucker@lunenfeld.ca).

Received 24 August; accepted 26 October; published online 7 December 2015 ; doi:10.1038/nm.3997

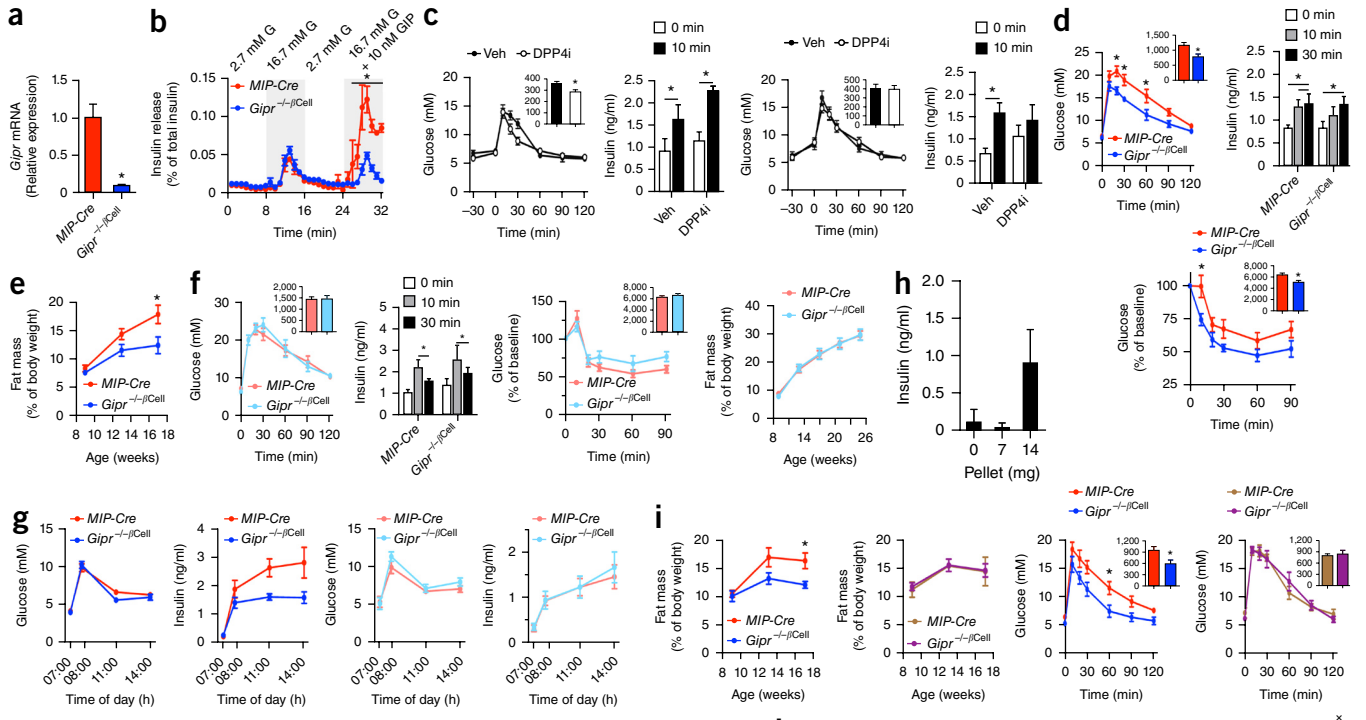

Figure 1 The phenotype of *Gipr*$^{-/-\beta\text{Cell}}$ mice. (**a**) *Gipr* expression in mouse islets ($n = 5$). (**b**) Insulin release from mouse islets from 18-week-old mice on LFD ($n = 7$). G, glucose. (**c**) Oral glucose tolerance test (OGTT) and plasma insulin levels in 12-week-old *MIP-Cre* (two left panels) and *Gipr*$^{-/-\beta\text{Cell}}$ (two right panels) mice administered vehicle (veh) or sitagliptin (a dipeptidyl peptidase-4 inhibitor; DPP4i) (*MIP-Cre*, $n = 5$; *Gipr*$^{-/-\beta\text{Cell}}$, $n = 9$). (**d**) Glycemic (left) and insulin (middle) response during OGTT, and glycemic (bottom) response during an insulin tolerance test (ITT), all in 18-week-old LFD mice ($n = 7$). (**e**) Magnetic resonance imaging (MRI) assessment in LFD-fed mice ($n = 7$). (**f**) Glycemic and insulin (two left panels) responses during OGTT, glycemic (middle right) response during ITT; MRI assessment (right) in 18-week-old HFD-fed mice (*MIP-Cre*, $n = 9$; and *Gipr*$^{-/-\beta\text{Cell}}$, $n = 13$). (**g**) Glycemic and insulin (left) responses to re-feeding in 10-week-old LFD-fed mice (*MIP-Cre*, $n = 6$; *Gipr*$^{-/-\beta\text{Cell}}$, $n = 9$). Glycemic and insulin (right) responses to refeeding in 10-week-old HFD-fed animals (*MIP-Cre*, $n = 8$; *Gipr*$^{-/-\beta\text{Cell}}$, $n = 13$). (**h**) Plasma insulin after a 16 h fast, after sham or after insulin pellet (7 or 14 mg) surgery ($n = 3$, 4 and 4, respectively). (**i**) MRI analysis (two left panels) after sham (left) or insulin (middle-left) pellet surgery. Glycemic levels (two right panels) during OGTT in 18-week-old mice without (middle-right) or with insulin (right) pellet ($n = 3$, 5, 3 and 6, respectively). (**j**) Glycemic (left) and insulin (middle) responses during an intraperitoneal glucose tolerance test (IPGTT) in 18-week-old HFD-mice given Ex4 (*MIP-Cre*, $n = 9$; *Gipr*$^{-/-\beta\text{Cell}}$, $n = 13$). Insulin secretion (right) from mouse islets isolated from 18-week-old LFD-fed mice ($n = 7$). $^*P < 0.05$ versus control, or as indicated. Data are expressed as mean ± s.e.m. Statistical tests used: *t*-test in **a** and AUC insets (**c**,**d**,**f**,**h**,**i**); two-way analysis of variance (ANOVA) for **b**–**g** and **i**,**j**.

glycemic excursion after glucose challenge in all three lines of control mice but did not lower glycemia in *Gipr*$^{-/-\beta\text{Cell}}$ mice (**Supplementary Fig. 1c**). GIP also robustly stimulated insulin secretion in perifused islets from control mice, but not in those from *Gipr*$^{-/-\beta\text{Cell}}$ mice (**Fig. 1b**). Administration of a low dose of a DPP4 inhibitor modestly improved glucose tolerance and enhanced glucose-stimulated insulin secretion in control mice but not in *Gipr*$^{-/-\beta\text{Cell}}$ mice (**Fig. 1c**). For subsequent experiments, we used *MIP-Cre* mice as controls, minimizing any potential confounding effects associated with Cre-driver lines in beta cells[14,15]. Notably, human growth hormone (hGH) release and expression of tryptophan hydroxylase-1 (*Tph1*) and -2 (*Tph2*) were similar in islets from *MIP-Cre* and from *Gipr*$^{-/-\beta\text{Cell}}$ mice (**Supplementary Fig. 1d**).

Although mice with whole-body deletion of *Gipr* exhibit modestly impaired beta cell function[10], 8-week-old *Gipr*$^{-/-\beta\text{Cell}}$ mice fed a low-fat diet (LFD) showed normal oral glucose tolerance and glucose-stimulated insulin levels (**Supplementary Fig. 1e**). Furthermore, insulin sensitivity, weight gain, ambient glycemia, food intake and plasma incretin levels were all comparable in *Gipr*$^{-/-\beta\text{Cell}}$ and *MIP-Cre* control mice (**Supplementary Fig. 1f–h**). Unexpectedly, oral and intraperitoneal glucose tolerance and insulin sensitivity were paradoxically better in 18-week-old *Gipr*$^{-/-\beta\text{Cell}}$ mice than in *MIP-Cre* controls (**Fig. 1d** and **Supplementary Fig. 1i**). *Gipr*$^{-/-\beta\text{Cell}}$ mice accumulated less white adipose tissue (WAT) with age and exhibited reduced adipocyte size (**Fig. 1e** and **Supplementary Fig. 2a**), despite having both similar expression levels of the genes that regulate adipose-tissue metabolism and comparable lipoprotein lipase activity in adipose tissue (**Supplementary Fig. 2b**,**c**).

We reasoned that GIPR-deficient beta cells produce less insulin than do beta cells with normal GIPR levels, which, in turn, limits expansion of WAT depots, thereby improving insulin sensitivity[16]. Accordingly, we reassessed these phenotypes by using two independent strategies to restore insulin levels: (i) exposure to a high-fat diet (HFD) and (ii) direct insulin replacement. A HFD stimulates GIP secretion, which will expand adipose tissue mass, increase both resistin expression and secretion and promote insulin resistance, thereby indirectly enhancing insulin secretion even in the absence of GIPR action in beta cells[17,18]. HFD-fed *Gipr*$^{-/-\beta\text{Cell}}$ mice exhibited weight

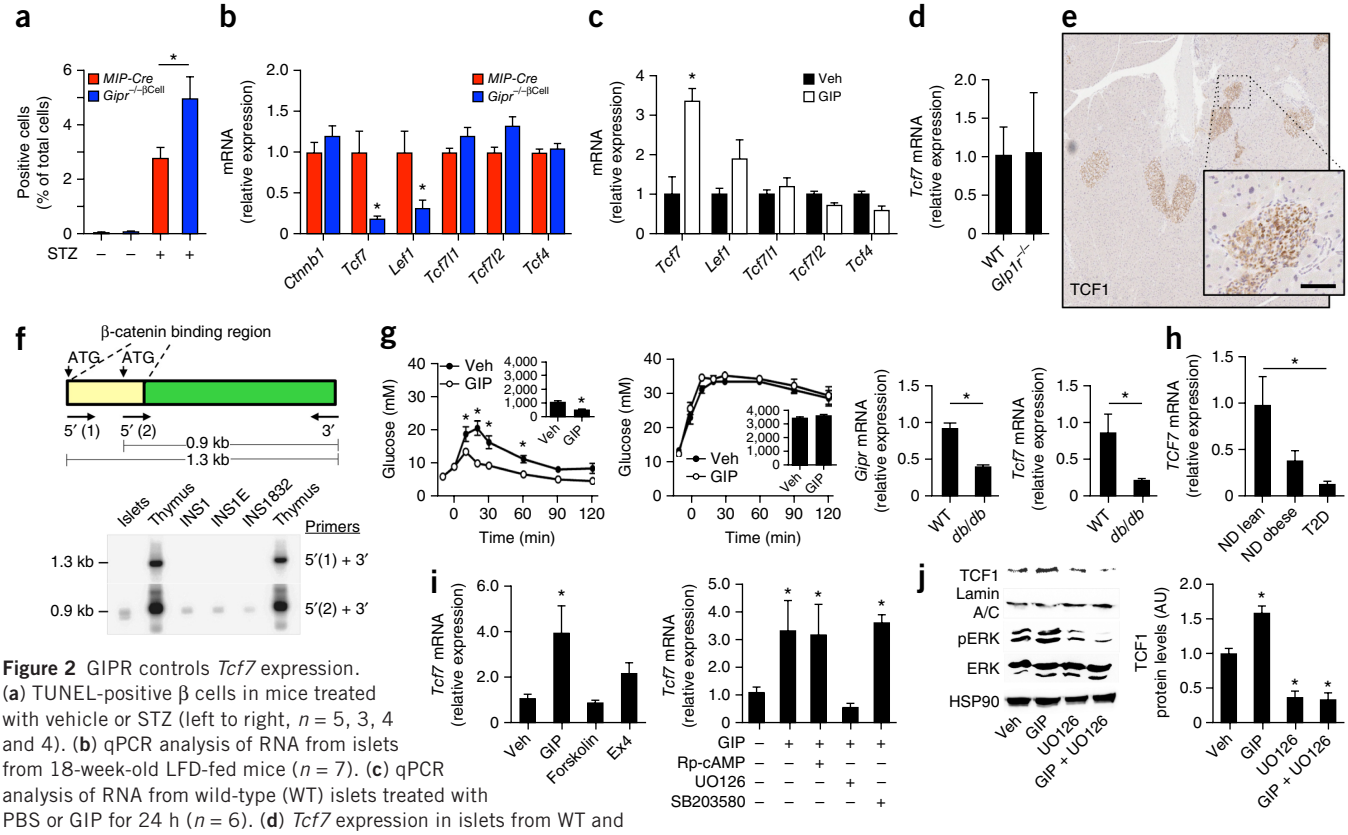

Figure 2 GIPR controls *Tcf7* expression. (**a**) TUNEL-positive β cells in mice treated with vehicle or STZ (left to right, $n = 5$, 3, 4 and 4). (**b**) qPCR analysis of RNA from islets from 18-week-old LFD-fed mice ($n = 7$). (**c**) qPCR analysis of RNA from wild-type (WT) islets treated with PBS or GIP for 24 h ($n = 6$). (**d**) *Tcf7* expression in islets from WT and *Glp1r*$^{-/-}$ mice ($n = 4$). (**e**) Representative image of immunohistochemistry for TCF1 expression in WT mouse pancreas. Scale bar, 50 µm ($n = 3$). (**f**) Schematic of the *Tcf7* mRNA coding region (top) demonstrating multiple start codons. Representative image (bottom) of 1.3 kb and 0.9 kb *Tcf7* PCR products from mouse islets and rat insulinoma cell (INS1) subclones INS1, INS1E and INS1832 ($n = 2$). (**g**) Glycemic response during an IPGTT in WT (left) and *db/db* (middle left) mice ($n = 5$). qPCR analysis for *Gipr* (middle right) and *Tcf7* (right) mRNA in mouse islets ($n = 5$). (**h**) *TCF7* expression in human islets ($n = 5$, 5 and 4). ND, non-diabetic. (**i**) *Tcf7* expression in WT mouse islet RNA (left, $n = 4$) or INS1 832/32 β cells (right, $n = 6$). (**j**) Tcf1, Lamin A/C, phosphorylated or non-phosphorylated extracellular signal–regulated kinase (ERK) and heat shock protein 90 (HSP90) protein expression in INS1 832/32 β cells ($n = 6$). $^*P < 0.05$ versus control or as indicated. Data are expressed as mean ± s.e.m. Statistical tests used: *t*-test for **b**–**d**,**g** (AUC insets); one-way analysis of variance (ANOVA) for **h**–**j**; two-way ANOVA for **a**,**g**. TUNEL, terminal deoxynucleotidyl transferase dUTP nick end labeling.

gain, plasma incretin levels and glycemia similar to those seen in *MIP-Cre* controls (**Supplementary Fig. 2d**), but they no longer exhibited improved glucose tolerance, higher insulin sensitivity or less adipose tissue mass as compared to *MIP-Cre* controls (**Fig. 1f** and **Supplementary Fig. 2d**).

Consistent with an essential role for the beta cell GIPR in nutrient-regulated insulin secretion, insulin levels were lower in LFD-fed *Gipr*$^{-/-\beta\text{Cell}}$ mice than in LFD-fed *MIP-Cre* mice during the re-feeding period after an overnight fast, despite showing comparable levels of glycemia (**Fig. 1g**). In contrast, HFD feeding restored insulin profiles in *Gipr*$^{-/-\beta\text{Cell}}$ mice to the levels observed in *MIP-Cre* mice (**Fig. 1g**). We next implanted insulin pellets in *Gipr*$^{-/-\beta\text{Cell}}$ mice to reverse the relative hypoinsulinemia detected under LFD conditions (**Fig. 1g**). The pellets raised insulin levels by ~1 ng per ml (**Fig. 1h**), an amount similar to the difference in postprandial insulin values detected in *MIP-Cre* compared to *Gipr*$^{-/-\beta\text{Cell}}$ mice (**Fig. 1g**); insulin pellets had no effect on body weight, glycemia (**Supplementary Fig. 2e**) or food intake (data not shown). The normalization of postprandial insulinemia restored adiposity and insulin sensitivity to control levels in *Gipr*$^{-/-\beta\text{Cell}}$ mice (**Fig. 1i** and **Supplementary Fig. 2f**).

The relatively modest basal glucose-tolerance phenotype of *Gipr*$^{-/-\beta\text{Cell}}$ mice may reflect the upregulation of related nutrient-sensitive beta cell signaling pathways[19–21]. Indeed *Gipr*$^{-/-\beta\text{Cell}}$ mice exhibited greater insulin secretion in response to the GLP-1R agonist exendin-4 (Ex4) *in vivo* and in isolated perifused islets *ex vivo* relative to *MIP-Cre* mice (**Fig. 1j**). Conversely, the selective reduction of GLP-1R signaling impaired glucose tolerance to a greater extent in *Gipr*$^{-/-\beta\text{Cell}}$ mice than in *MIP-Cre* controls (**Supplementary Fig. 2g**). Similarly, individual patch-clamped beta cells from *Gipr*$^{-/-\beta\text{Cell}}$ mice did not respond to GIP yet exhibited enhanced sensitivity to Ex4 (**Supplementary Fig. 2h**), whereas beta cells from *Gipr*$^{-/-\beta\text{Cell}}$ mice demonstrated normal actin-depolymerization responses to high levels of either glucose or Ex4 but did not respond to GIP (**Supplementary Fig. 2i**). *Gipr*$^{-/-\beta\text{Cell}}$ mice also exhibited enhanced sensitivity to exogenous administration of the insulinotropic G protein–coupled receptor (GPCR) 119 (GPR119) agonist AR231453 compared to control mice (**Supplementary Fig. 2j**).

Given that class B GPCRs modulate beta cell growth and survival[1,22], we analyzed *Gipr*$^{-/-\beta\text{Cell}}$ islets. Loss of the beta cell GIPR reduced beta cell area, but islet size, islet number, granule morphology and granule size were all unaffected (**Supplementary Fig. 3a**,**b**). The adaptive increase in beta cell mass after exposure to a HFD was preserved in *Gipr*$^{-/-\beta\text{Cell}}$ mice (**Supplementary Fig. 3a**), revealing that the beta cell GIPR is dispensable for the adaptive response to insulin resistance. Because GIPR signaling controls beta cell survival[23,24], we assessed the response to the beta cell toxin streptozotocin (STZ).

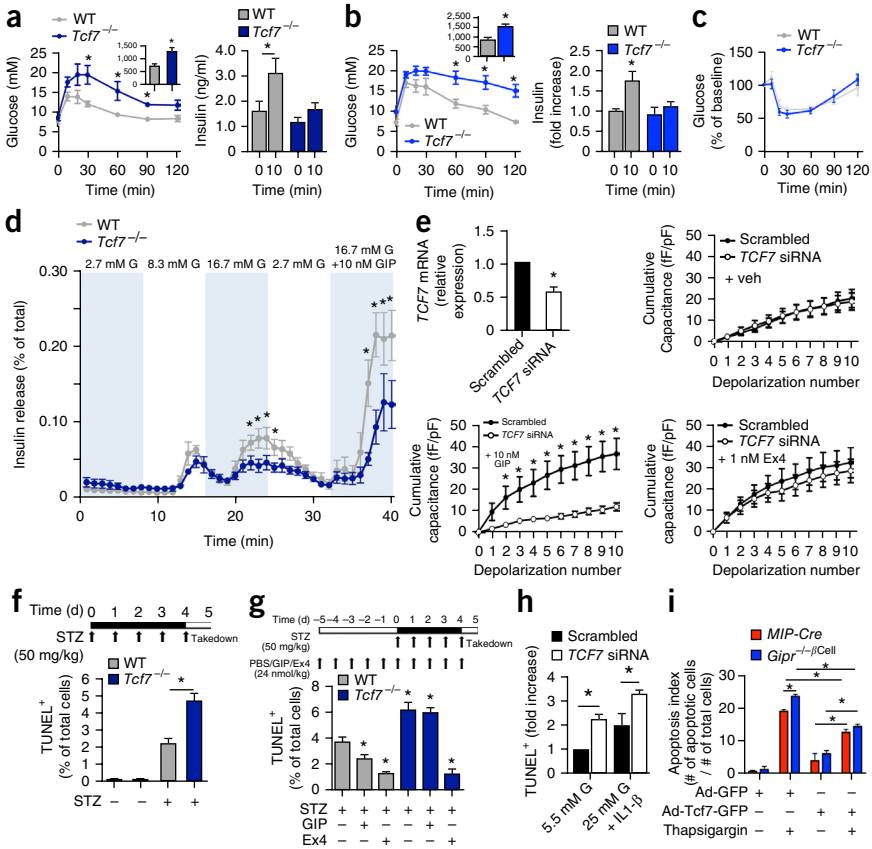

Figure 3 Phenotype of *Tcf7*$^{-/-}$ mice. (**a**) Glycemic (left) and insulin (right) response during an OGTT in 18-week-old mice fed a LFD ($n = 7$ and 8). (**b**) Glycemic (left) and insulin (right) response during an OGTT in 12-week-old HFD-fed mice ($n = 4$ and 8). (**c**) Glycemic response during an intraperitoneal insulin tolerance test (ITT) in 12-week-old HFD-fed mice ($n = 5$). (**d**) Insulin release from islets isolated from 18-week-old LFD-fed mice ($n = 8$). (**e**) *TCF7* expression in beta cells from human donors (top left) ($n = 4$ and 4). Cumulative capacitance during sequential depolarization in individual human beta cells exposed to veh (top right, $n = 16$ and 18), GIP (bottom left, $n = 15$ and 15) or Ex4 (bottom right, $n = 14$ and 13). (**f**) TUNEL-positive beta cells in mice treated with veh or STZ ($n = 5$, 4, 4 and 5). (**g**) TUNEL-positive beta cells in mice treated with STZ plus veh, GIP, or Ex4 ($n = 4$). (**h**) TUNEL-positive staining in human beta cells (several hundred cells from four individual donors) treated with low (5.5 mM) glucose (G) or high (25 mM) G plus interleukin 1-β (IL-1β). (**i**) Apoptotic index in mouse beta cells ($n = 3$ for *MIP-Cre* and 5 for *Gipr*$^{-/-\beta Cell}$). $^*P < 0.05$ versus control, or as indicated. Data are expressed as mean ± s.e.m. Statistical tests used: *t*-test for **e** (top left) and AUC insets (**a**,**b**); two-way ANOVA for **a**–**i**.

More apoptotic beta cells were detected in islets from STZ-treated *Gipr*$^{-/-\beta Cell}$ mice than in those from *MIP-Cre* controls (**Fig. 2a**), whereas levels of mRNA transcripts for genes encoding either pro-survival GPCRs, components of the glucose-sensing machinery, including GLUT2 (*Slc2a2*, which transports STZ), and mediators of proliferation or survival were not differentially expressed in *Gipr*$^{-/-\beta Cell}$ islets (**Supplementary Fig. 3c** and **Supplementary Table 1**).

As the Wnt target *TCF7L2* regulates both incretin-receptor expression and beta cell survival[8,25], we assessed mRNA levels of β-catenin and members of the TCF family. Islet expression levels of catenin (cadherin-associated protein), beta 1 (*Ctnnb1*), *Tcf7l1*, *Tcf7l2* and *Tcf4* were not affected by a loss of GIPR in beta cells; however, mRNA transcripts for *Tcf7* and for lymphoid enhancer binding factor 1 (*Lef1*), both of which encode proteins not previously assigned functional roles in beta cells, were markedly lower in *Gipr*$^{-/-\beta Cell}$ islets (**Fig. 2b**). Moreover, GIP directly increased *Tcf7* expression in WT mouse islets *ex vivo* (**Fig. 2c**). Furthermore, although GLP-1R and GIPR share cAMP-dependent pathways[26] to regulate beta cell function and survival[27], *Tcf7* expression was not perturbed in islets from *Glp1r*$^{-/-}$ mice (**Fig. 2d**).

Immunohistochemistry localized Tcf1 (the protein product of *Tcf7*) to mouse islets (**Fig. 2e** and **Supplementary Table 2**). *Tcf7* has been principally studied in immune cells, wherein alternative promoter utilization and RNA splicing[28] gives rise to multiple RNA transcripts, including two major transcripts (~1.3 kb and ~0.9 kb) in the thymus (**Fig. 2f**). The dominant *Tcf7* mRNA transcript detected in mouse islets and beta cell lines was ~0.9 kb (**Fig. 2f**) and was absent in *Tcf7*$^{-/-}$ islets (**Supplementary Fig. 3d**). GIP directly induced *Tcf7* expression in the rat insulin-secreting (INS-1) beta cell line, and in human islets (*TCF7*) (**Supplementary Fig. 3e**,**f**). Although GIP lowered glycemia in WT control mice, 12-week-old, obese, diabetic *db/db* mice displayed significantly lower islet levels of *Tcf7* and *Gipr* mRNA transcripts and did not lower their glucose levels or secrete insulin in response to exogenous GIP (**Fig. 2g** and **Supplementary Fig. 4a–d**). By contrast, the levels of *Glp1r* and *Tcf7l2* mRNA transcripts were unchanged in islet RNA from 6- or 12-week-old *db/db* mice (**Supplementary Fig. 4e**). Levels of *TCF7* mRNA transcripts were lower in islets from obese, non-diabetic subjects and significantly lower in islets from subjects with T2D than in non-obese, non-diabetic control subjects (**Fig. 2h** and **Supplementary Fig. 4f**). The GIP-dependent induction of *Tcf7* expression was not mimicked by forskolin or by Ex4 and was not sensitive to the cAMP-inhibitor Rp-cAMP (**Fig. 2i**). By contrast, the inhibition of ERK1/2 phosphorylation with the mitogen-activated protein kinase inhibitor UO126 completely prevented the GIP-stimulated increase in *Tcf7* RNA (**Fig. 2i**) and Tcf1 protein levels (**Fig. 2j**). Hence signaling via the GIPR, but not the GLP-1R, controls *Tcf7*/Tcf1 expression through a cAMP-independent and ERK1/2-dependent pathway in beta cells.

To identify a role for Tcf1 in beta cells, we studied *Tcf7*$^{-/-}$ mice. Body weight and fat mass were similar in WT mice and *Tcf7*$^{-/-}$ mice maintained on a LFD or HFD (**Supplementary Fig. 5a**,**b**). Glucose tolerance and plasma insulin levels were normal in 8-week-old *Tcf7*$^{-/-}$ mice on a LFD (**Supplementary Fig. 5c**). However, intraperitoneal glucose tolerance was profoundly impaired, and the insulin response to glucose was markedly attenuated, in older (18-week-old) *Tcf7*$^{-/-}$ mice on a LFD (**Fig. 3a**). Both oral and intraperitoneal glucose tolerance were severely impaired after only 4 weeks of HFD feeding because of the defective upregulation of glucose-stimulated insulin levels (**Fig. 3b** and **Supplementary Fig. 5d**), whereas sensitivity to exogenous insulin was comparable in WT and *Tcf7*$^{-/-}$ mice (**Fig. 3c**). Isolated islets from *Tcf7*$^{-/-}$ mice displayed significantly impaired insulin release in response to glucose and GIP (**Fig. 3d**). Similarly to islets from *Gipr*$^{-/-\beta Cell}$ mice, *Tcf7*$^{-/-}$ beta cells failed to respond to GIP yet demonstrated enhanced sensitivity to Ex4 (**Supplementary Fig. 5e**).

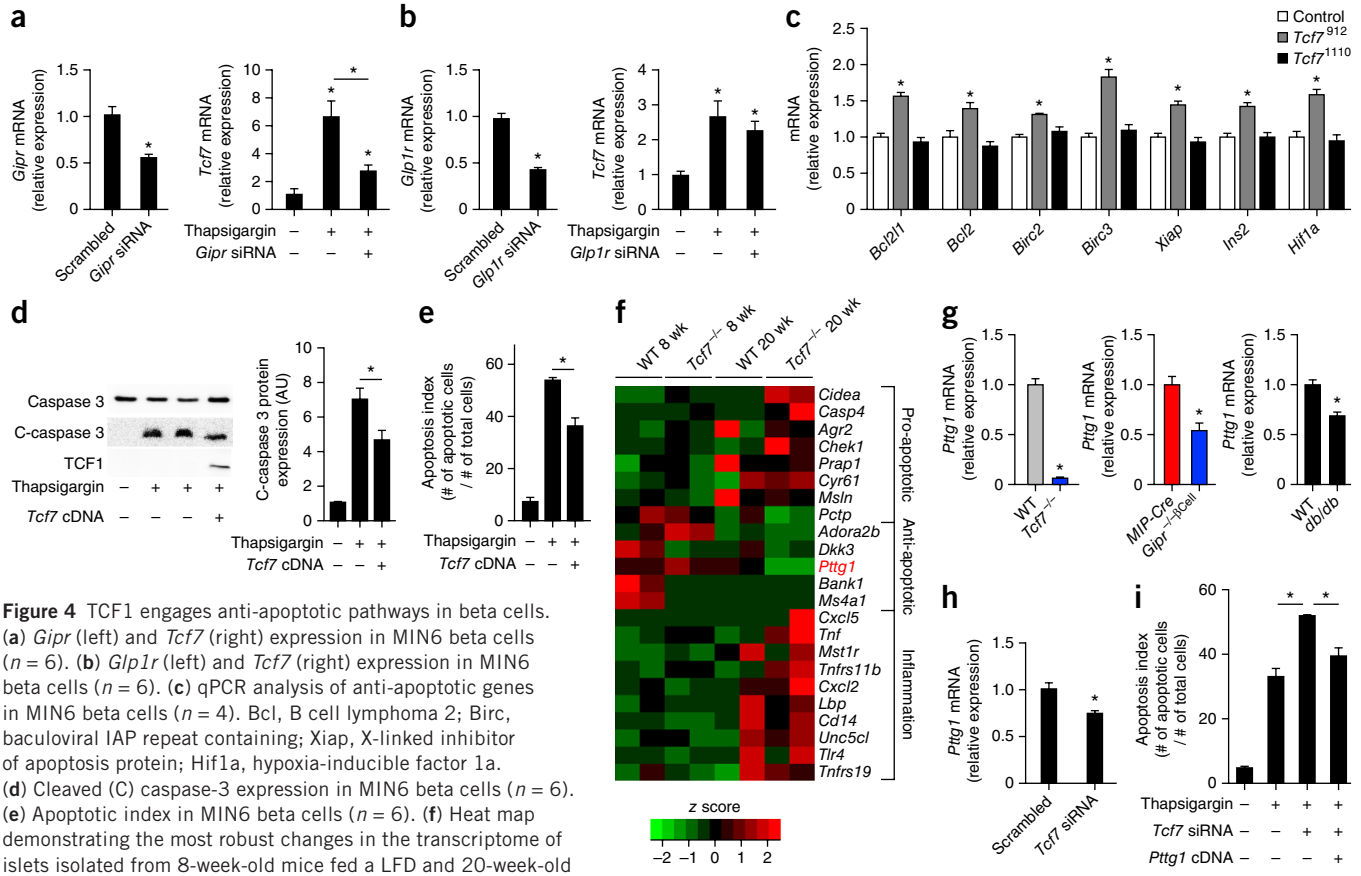

Figure 4 TCF1 engages anti-apoptotic pathways in beta cells. (**a**) *Gipr* (left) and *Tcf7* (right) expression in MIN6 beta cells ($n = 6$). (**b**) *Glp1r* (left) and *Tcf7* (right) expression in MIN6 beta cells ($n = 6$). (**c**) qPCR analysis of anti-apoptotic genes in MIN6 beta cells ($n = 4$). Bcl, B cell lymphoma 2; Birc, baculoviral IAP repeat containing; Xiap, X-linked inhibitor of apoptosis protein; Hif1a, hypoxia-inducible factor 1a. (**d**) Cleaved (C) caspase-3 expression in MIN6 beta cells ($n = 6$). (**e**) Apoptotic index in MIN6 beta cells ($n = 6$). (**f**) Heat map demonstrating the most robust changes in the transcriptome of islets isolated from 8-week-old mice fed a LFD and 20-week-old mice fed a HFD ($n = 2$). (**g**) *Pttg1* expression in RNA isolated from mouse islets from 20-week-old HFD-fed mice (left, $n = 4$), 18-week-old LFD-fed mice (middle, $n = 7$) and 12-week-old mice on standard rodent chow (right, $n = 5$). (**h**) *Pttg1* expression in MIN6 beta cells ($n = 6$). (**i**) Apoptotic index in MIN6 beta cells ($n = 6$). $^*P < 0.05$ vs control, or as indicated. Data are expressed as mean ± s.e.m. Statistical tests used: *t*-test for **a** (left), **b** (left), **g**,**h**; one-way analysis of variance (ANOVA) for **a** (right), **b** (right), **c**–**e**,**i**.

Furthermore, knockdown of *TCF7* in human beta cells produced a defective exocytosis response to GIP but not to Ex4 (**Fig. 3e**). Consistent with findings in $Gipr^{-/-\beta Cell}$ islets, $Tcf7^{-/-}$ islets showed no significant differences in their expression of genes encoding pro-survival GPCRs, components of the glucose-sensing machinery, mediators of proliferation or survival, or members of the TCF family (**Supplementary Fig. 5f**). Unlike findings for $Gipr^{-/-\beta Cell}$ mice, both LFD- and HFD-fed $Tcf7^{-/-}$ mice demonstrated normal glycemia and insulin release in response to refeeding after an overnight fast (**Supplementary Fig. 5g**). However, histological analysis of $Tcf7^{-/-}$ pancreata revealed an increase in beta cell mass after HFD feeding compared to that in WT controls (**Supplementary Fig. 5h**), comparable to findings in $Gipr^{-/-\beta Cell}$ mice (**Supplementary Fig. 3a**). Furthermore, $Tcf7^{-/-}$ mice on either a LFD or a HFD demonstrated reduced glycemia in response to the administration of DPP4 inhibitors or incretin-receptor agonists (**Supplementary Fig. 6a–d**). Thus, $Tcf7^{-/-}$ mice recapitulate many, but not all, of the metabolic phenotypes that are evident in $Gipr^{-/-\beta Cell}$ mice.

Given that TCF1 controls thymocyte survival[29], and that $Gipr^{-/-\beta Cell}$ mice demonstrate enhanced sensitivity to beta cell apoptosis, we assessed apoptotic injury in $Tcf7^{-/-}$ beta cells. Notably, $Tcf7^{-/-}$ islets exhibited a greater number of apoptotic beta cells after STZ administration than did WT islets (**Fig. 3f**). Furthermore, GIP reduced apoptosis in the islets of STZ-treated WT mice but not in islets from $Tcf7^{-/-}$ mice (**Fig. 3g**). By contrast, Ex4 significantly reduced islet apoptosis in both STZ-treated WT and STZ-treated $Tcf7^{-/-}$ mice (**Fig. 3g**). Knockdown of *TCF7* in human islet cells increased the number of apoptotic cells in islets cultured either in low glucose alone or in 25 mM of glucose with interleukin 1–β (**Fig. 3h**). Rescue of Tcf1 levels in dispersed islets from $Gipr^{-/-\beta Cell}$ mice lowered apoptotic rates (after thapsigargin administration) to levels comparable to those detected in WT controls (**Fig. 3i** and **Supplementary Fig. 7**).

The induction of apoptosis by administration of thapsigargin enhanced *Tcf7* expression in mouse insulinoma 6 (MIN6) beta cells, which was significantly attenuated by knockdown of the *Gipr*, but not of the *Glp1r* (**Fig. 4a**,**b**). The transfection of MIN6 beta cells with cDNAs encoding the single TCF1 protein, $Tcf7^{912}$ (the isoform expressed in mouse islets), increased the expression of anti-apoptotic genes (**Fig. 4c**) and reduced thapsigargin-stimulated caspase-3 cleavage and apoptosis (**Fig. 4d**,**e** and **Supplementary Fig. 8a**).

To further elucidate the consequences of TCF1-deficiency in beta cells, we performed RNA-seq analysis on islets from young, metabolically healthy (8-week-old, LFD) mice, older, obese (20-week-old, HFD) $Tcf7^{-/-}$ mice and littermate control mice. Robust changes in genes important for apoptosis and inflammation are detected in RNA from the islets of older $Tcf7^{-/-}$ mice (**Fig. 4f**). Notably, expression of pituitary tumor–transforming gene 1 (*Pttg1*), which encodes securin, a protein that regulates chromosome stability and DNA repair[30], was virtually absent in islet RNA from older $Tcf7^{-/-}$ mice (**Fig. 4g**). *Pttg1* expression was also significantly reduced both in RNA from $Gipr^{-/-\beta Cell}$ islets (**Fig. 4g**) and in islet RNA (**Fig. 4g**) from 12-week-old, diabetic *db/db* mice that exhibit reduced expression of *Gipr* and *Tcf7* (**Fig. 2g**).

These results are consistent with a GIPR-TCF1-PTTG1 axis. Finally, knockdown of *Tcf7* mRNA transcripts in MIN6 beta cells (**Supplementary Fig. 8b**) led to a significant reduction in *Pttg1* expression (**Fig. 4h**), whereas the restoration of *Pttg1* expression attenuated the increased susceptibility to apoptosis in MIN6 beta cells seen after *Tcf7* knockdown (**Fig. 4i**).

Taken together, these results greatly extend our understanding of incretin action and beta cell function and have direct translational implications. Previous findings that *Gipr*$^{-/-}$ mice are protected against diet-induced obesity and insulin resistance, coupled with genetic linkage of variants in the human *GIPR* to body weight[3], were attributed to GIP action in adipose tissue. The relatively modest differences in glucose tolerance arising from the selective loss of GIPR signaling in beta cells is ameliorated in part by compensatory increases in the activity of functionally related beta cell GPCRs. Nevertheless, our data demonstrate that the selective attenuation of GIP action in beta cells limits meal-related insulin release, indirectly reducing the expansion of adipose tissue mass and leading to improvements in insulin sensitivity and glucose tolerance. These findings support observations linking variation in the human *GIPR* gene with reduced insulin secretion and decreased body mass index[31], necessitating reconsideration of the importance of direct versus indirect GIP action in beta cells compared to that in adipocytes for the control of insulin sensitivity and adipose tissue mass.

Although GLP-1 and GIP exert their actions through structurally and functionally related incretin receptors[1,22], our findings that GIPR, but not GLP-1R, signaling controls *Tcf7* expression independently of cAMP signaling identify divergent downstream signaling pathways that link incretin-receptor signaling to beta cell survival. Indeed, the loss of GLP-1R, but not of GIPR, signaling, impairs expression of insulin receptor substrate 2 (*Irs2*) in mouse islets[18], and beta cells from *Glp1r*$^{-/-}$ mice exhibit greater sensitivity to STZ-induced apoptotic injury than *Gipr*$^{-/-}$ beta cells[24]. Furthermore, GIP, but not GLP-1, controls osteopontin expression in mouse islets[31], whereas GLP-1R, but not GIPR, signaling is essential for the adaptive islet response to pregnancy. Our identification of a GIPR-TCF1 axis uncovers a novel mechanistic pathway linking differential incretin-receptor signaling to the control of beta cell mass and function, which has encouraging implications for therapeutic strategies based on GIPR agonism.

Considerable evidence from human genetic and physiological studies has linked variation within the human *TCF7L2* gene to impairment of beta cell function and an increased risk of developing T2D[32,33]. Nevertheless, our understanding of how TCF7L2 controls beta cell function has been challenged by studies demonstrating that genetic inactivation of the *Tcf7l2* gene in beta cells does not impair beta cell function[34], whereas enhanced *Tcf7l2* expression (TCF4) in liver activated a metabolic gene-expression program linked to increased hepatic glucose output[34]. This suggests that TCF4 may indirectly affect beta cell function through hepatic Wnt signaling. Tcf1 is deficient in the hepatocytes of diabetic mice, and restoring *Tcf7* expression reduces gluconeogenesis[35], further positioning *Tcf7* in the pathophysiology of diabetes. Collectively, our findings demonstrated that *Tcf7*/Tcf1 is required for maintaining beta cell survival and that the disruption of *Tcf7* (loss of Tcf1) unmasks divergent mechanisms regulating the anti-apoptotic actions of GIPR as compared to GLP-1R signaling in mouse islets. In contrast to conflicting data surrounding the role of TCF7L2 in beta cells, our latest data unequivocally reveal the importance of *Tcf7*/Tcf1, regulated by GIPR signaling, for the direct control of beta cell survival in murine and human islets.

Levels of *Tcf7* mRNA transcripts are reduced in the pancreas from HFD-fed rats[36], and variation in the human *TCF7* gene has been linked to an increased risk for development of type 1 diabetes[37,38]; whether these latter findings reflect TCF1-dependent disturbances of immune regulation, beta cell function or beta cell survival in susceptible individuals requires further investigation. Moreover, the importance of the TCF1 target, PTTG1, for beta cell function and survival has been independently shown in studies of older *Pttg1*$^{-/-}$ mice, which exhibited reduced beta cell mass, impaired beta cell function and increased beta cell apoptosis[39,40].

Our current data establish that TCF1, acting through PTTG1, links GIPR signaling to the control of insulin secretion, the survival of beta cells and the adaptation of these cells to metabolic stress. Given that GIPR, but not GLP-1R, signaling controlled the TCF1-PTTG1 axis in beta cells, and that GIP responsiveness was rapidly restored after a brief period of improved glucose control in human subjects with T2D[13], our findings highlight the potential of targeting GIPR-TCF1-PTTG1 signaling for the preservation of beta cell mass and the treatment of diabetes. Collectively, our data imply that the development of GIP-based therapies may target novel pathways, independently of GLP-1R signaling, thus linking nutrient-activated signals to the control of beta cell function and survival.

METHODS

Methods and any associated references are available in the online version of the paper.

Accession codes. RNA-seq data has been deposited with accession code GSE65361.

Note: Any Supplementary Information and Source Data files are available in the online version of the paper.

ACKNOWLEDGMENTS

The authors thank H. Bates for excellent technical assistance and B. Yusta for thoughtful discussions and critical reading of the manuscript; H. Clevers for *Tcf7*$^{-/-}$ mice; and R. DiMarchi for critical reagents. This work in Toronto was supported by the Canada Research Chairs Program, the Banting and Best Diabetes Centre Novo Nordisk Chair in Incretin Biology, and Canadian Institute for Health Research (CIHR) grants 82700 and 123391 (DJD). We thank the Human Organ Procurement and Exchange (HOPE) program and the Trillium Gift of Life Network (TGLN) for their assistance in obtaining pancreases and islets from human organ donors for research, and we thank J. Lyon (Alberta Diabetes Institute; http://www.bcell.org/isletcore.html) and T. Kin and A.M.J. Shapiro (University of Alberta, Clinical Islet Isolation Facility) for human islet isolation. The Alberta Diabetes Foundation funded the human islet isolations. Work at the University of Alberta was funded by a grant from the Canadian Diabetes Association (to P.E.M.). P.E.M. holds a Canada Research Chair in Islet Biology. Postdoctoral fellowship funding was provided by the Canadian Institute for Health Research (J.E.C., J.R.U., and E.E.M.), Banting and Best Diabetes Centre (J.E.C.), the Canadian Diabetes Association (E.E.M.) and Alberta Innovates Health Solutions (J.R.U.). D.J.D. is the main guarantor of this work and takes responsibility for all content.

AUTHOR CONTRIBUTIONS

J.E.C. and D.J.D. designed and directed the study, analyzed data and wrote the manuscript. J.R.U., E.E.M., L.L.B. and P.E.M. contributed to the study design and the preparation of the manuscript. J.E.C., J.R.U., E.E.M., J.K., L.L.B., X.C., B.J.L. and T.M. performed experiments. J.K. and P.E.M. carried out experiments on human islets. Y.L. and J.L.W. provided assistance with the RNA-seq data. N.T. and L.H.P. provided *MIP-Cre* mice. C.J.S. performed the electron microscopy. All authors reviewed the manuscript and provided final approval for submission.

COMPETING FINANCIAL INTERESTS

The authors declare competing financial interests: details are available in the online version of the paper.

1. Campbell, J.E. & Drucker, D.J. Pharmacology physiology and mechanisms of incretin hormone action. *Cell Metab.* **17**, 819–837 (2013).
2. Saxena, R. *et al.* Genetic variation in GIPR influences the glucose and insulin responses to an oral glucose challenge. *Nat. Genet.* **42**, 142–148 (2010).
3. Speliotes, E.K. *et al.* Association analyses of 249,796 individuals reveal 18 new loci associated with body mass index. *Nat. Genet.* **42**, 937–948 (2010).
4. Miyawaki, K. *et al.* Inhibition of gastric inhibitory polypeptide signaling prevents obesity. *Nat. Med.* **8**, 738–742 (2002).
5. Mulvihill, E.E. & Drucker, D.J. Pharmacology, physiology and mechanisms of action of dipeptidyl peptidase-4 inhibitors. *Endocr. Rev.* **35**, 992–1019 (2014).
6. Finan, B. *et al.* Unimolecular dual incretins maximize metabolic benefits in rodents, monkeys and humans. *Sci. Transl. Med.* **5**, 209ra151 (2013).
7. Finan, B. *et al.* A rationally designed monomeric peptide triagonist corrects obesity and diabetes in rodents. *Nat. Med.* **21**, 27–36 (2015).
8. Shu, L. *et al.* Decreased TCF7L2 protein levels in type 2 diabetes mellitus correlate with downregulation of GIP- and GLP-1 receptors and impaired beta-cell function. *Hum. Mol. Genet.* **18**, 2388–2399 (2009).
9. Wessel, J. *et al.* Low-frequency and rare exome chip variants associate with fasting glucose and type 2 diabetes susceptibility. *Nat. Commun.* **6**, 5897 (2015).
10. Miyawaki, K. *et al.* Glucose intolerance caused by a defect in the entero-insular axis: a study in gastric inhibitory polypeptide receptor knockout mice. *Proc. Natl. Acad. Sci. USA* **96**, 14843–14847 (1999).
11. Meier, J.J. GLP-1 receptor agonists for individualized treatment of type 2 diabetes mellitus. *Nat. Rev. Endocrinol.* **8**, 728–742 (2012).
12. Nauck, M.A. *et al.* Preserved incretin activity of glucagon-like peptide 1 [7–36 amide] but not of synthetic human gastric inhibitory polypeptide in patients with type-2 diabetes mellitus. *J. Clin. Invest.* **91**, 301–307 (1993).
13. Højberg, P.V. *et al.* Four weeks of near-normalisation of blood glucose improves the insulin response to glucagon-like peptide-1 and glucose-dependent insulinotropic polypeptide in patients with type 2 diabetes. *Diabetologia* **52**, 199–207 (2009).
14. Brouwers, B. *et al.* Impaired islet function in commonly used transgenic mouse lines due to human growth hormone minigene expression. *Cell Metab.* **20**, 979–990 (2014).
15. Oropeza, D. *et al.* Phenotypic characterization of MIP-CreERT1Lphi mice with transgene-driven islet expression of human growth hormone. *Diabetes* **64**, 3798–3807 (2015).
16. Mehran, A.E. *et al.* Hyperinsulinemia drives diet-induced obesity independently of brain insulin production. *Cell Metab.* **16**, 723–737 (2012).
17. Chen, S., Okahara, F., Osaki, N. & Shimotoyodome, A. Increased GIP signaling induces adipose inflammation via a HIF-1alpha-dependent pathway and impairs insulin sensitivity in mice. *Am. J. Physiol. Endocrinol. Metab.* **308**, E414–E425 (2015).
18. Lamont, B.J. & Drucker, D.J. Differential anti-diabetic efficacy of incretin agonists vs. DPP-4 inhibition in high fat fed mice. *Diabetes* **57**, 190–198 (2008).
19. Ali, S., Lamont, B.J., Charron, M.J. & Drucker, D.J. Dual elimination of the glucagon and GLP-1 receptors in mice reveals plasticity in the incretin axis. *J. Clin. Invest.* **121**, 1917–1929 (2011).
20. Pamir, N. *et al.* Glucose-dependent insulinotropic polypeptide receptor null mice exhibit compensatory changes in the enteroinsular axis. *Am. J. Physiol. Endocrinol. Metab.* **284**, E931–E939 (2003).
21. Pederson, R.A. *et al.* Enhanced glucose-dependent insulinotropic polypeptide secretion and insulinotropic action in glucagon-like peptide 1 receptor –/– mice. *Diabetes* **47**, 1046–1052 (1998).
22. Mayo, K.E. *et al.* International Union of Pharmacology. XXXV. The glucagon receptor family. *Pharmacol. Rev.* **55**, 167–194 (2003).
23. Kim, S.J. *et al.* GIP stimulation of pancreatic beta-cell survival is dependent upon phosphatidylinositol 3-kinase (PI3-K)/ protein kinase B (PKB) signaling, inactivation of the Forkhead transcription factor Foxo1 and downregulation of bax expression. *J. Biol. Chem.* **280**, 22297–22307 (2005).
24. Maida, A., Hansotia, T., Longuet, C., Seino, Y. & Drucker, D.J. Differential importance of GIP versus GLP-1 receptor signaling for beta cell survival in mice. *Gastroenterology* **137**, 2146–2157 (2009).
25. Shu, L. *et al.* Transcription factor 7-like 2 regulates beta-cell survival and function in human pancreatic islets. *Diabetes* **57**, 645–653 (2008).
26. Yusta, B. *et al.* GLP-1 receptor activation improves β-cell function and survival following induction of endoplasmic reticulum stress. *Cell Metab.* **4**, 391–406 (2006).
27. Li, Y. *et al.* Glucagon-like peptide-1 receptor signaling modulates beta cell apoptosis. *J. Biol. Chem.* **278**, 471–478 (2003).
28. Van de Wetering, M., Castrop, J., Korinek, V. & Clevers, H. Extensive alternative splicing and dual promoter usage generate Tcf-1 protein isoforms with differential transcription control properties. *Mol. Cell. Biol.* **16**, 745–752 (1996).
29. Ioannidis, V., Beermann, F., Clevers, H. & Held, W. The beta-catenin–TCF-1 pathway ensures $CD4^+CD8^+$ thymocyte survival. *Nat. Immunol.* **2**, 691–697 (2001).
30. Vlotides, G., Eigler, T. & Melmed, S. Pituitary tumor-transforming gene: physiology and implications for tumorigenesis. *Endocr. Rev.* **28**, 165–186 (2007).
31. Lyssenko, V. *et al.* Pleiotropic effects of GIP on islet function involves osteopontin. *Diabetes* **60**, 2424–2433 (2011).
32. Grant, S.F. *et al.* Variant of transcription factor 7-like 2 (TCF7L2) gene confers risk of type 2 diabetes. *Nat. Genet.* **38**, 320–323 (2006).
33. Florez, J.C. *et al.* TCF7L2 polymorphisms and progression to diabetes in the Diabetes Prevention Program. *N. Engl. J. Med.* **355**, 241–250 (2006).
34. Boj, S.F. *et al.* Diabetes risk gene and Wnt effector Tcf7l2/TCF4 controls hepatic response to perinatal and adult metabolic demand. *Cell* **151**, 1595–1607 (2012).
35. Kaur, K. *et al.* Elevated hepatic miR-22–3p expression impairs gluconeogenesis by silencing the Wnt-responsive transcription factor, Tcf7. *Diabetes* **64**, 3659–3669 (2015).
36. Columbus, J. *et al.* Insulin treatment and high-fat diet feeding reduces the expression of three Tcf genes in rodent pancreas. *J. Endocrinol.* **207**, 77–86 (2010).
37. Noble, J.A. *et al.* A polymorphism in the TCF7 gene, *C883A*, is associated with type 1 diabetes. *Diabetes* **52**, 1579–1582 (2003).
38. Erlich, H.A., Valdes, A.M., Julier, C., Mirel, D. & Noble, J.A. Evidence for association of the TCF7 locus with type I diabetes. *Genes Immun.* **10** (suppl. 1), S54–S59 (2009).
39. Wang, Z., Moro, E., Kovacs, K., Yu, R. & Melmed, S. Pituitary tumor transforming gene-null male mice exhibit impaired pancreatic beta cell proliferation and diabetes. *Proc. Natl. Acad. Sci. USA* **100**, 3428–3432 (2003).
40. Chesnokova, V. *et al.* Diminished pancreatic beta-cell mass in securin-null mice is caused by beta-cell apoptosis and senescence. *Endocrinology* **150**, 10 (suppl. 1) 2603–2610 (2009).

COMPETING FINANCIAL INTERESTS

D.J.D. has been a consultant to Novo Nordisk Inc. and other companies that develop and/or sell incretin-based therapies, including Arisaph Pharmaceuticals Inc., Intarcia Therapeutics, Merck Research Laboratories, MedImmune, Receptos, Sanofi, Takeda and Transition Pharmaceuticals Inc. Neither D.J.D. nor his family members hold stock directly or indirectly in any of these companies.

EDITORIAL SUMMARY

AOP: The details of the GIP signaling pathway are murky, but new data identify a downstream pathway involving Tcf7 that regulates beta cell survival and activity.

ONLINE METHODS

Animals. Male mice were used for all mouse studies and were maintained under a 12 h light/12 h dark cycle at constant temperature (23 °C) with free access to food and water. All animal studies were approved by Mt. Sinai Hospital (Toronto) and the Toronto Centre for Phenogenomics animal-care committee. Animals were fed either a low-fat diet (10% kcal from fat; Research Diets, D12450B) or high-fat diet (45% kcal from fat; Research Diets, D12451). To generate $Gipr^{-/-\beta Cell}$ mice, MIPcreER transgenic mice (on a C57BL/6J background) expressing tamoxifen-inducible Cre driven by the mouse insulin promoter were bred with floxed *Gipr* mice ($Gipr^{Flox/Flox}$), backcrossed 8 times to C57BL/6J background)[41]. Cre-induced inactivation of the *Gipr* gene was carried out via 5 consecutive daily intraperitoneal (*i.p.*) injections of tamoxifen (40 mg per kg) in 6-week-old mice. $Glp1r^{-/-}$ and $Tcf7^{-/-}$ mice (both on C57BL/6J backgrounds) have been previously described[42,43]. $Tcf7^{-/-}$ mice were generously provided by H. Clevers, *db/db* mice were purchased from Jackson laboratories (#000697). For all animal experiments, the sample size required to achieve adequate power was estimated on the basis of pilot work or previous experiments. When appropriate, animals were randomly allocated to individual experimental groups.

Peptides and reagents. Peptides were reconstituted in phosphate-buffered saline (PBS), aliquoted and stored at −80 °C. [D-Ala^2]GIP (GIP) was from Chi Scientific, Ex4 (exendin-4) was from California Peptide Research Inc. Plasmid constructs (*Tcf7* and *Pttg1*) and siRNA (*Gipr*, *Glp1r*, *Tcf7, TCF7*) were from Origene. The GLP-1R antagonist (JANT-4)[44] was a generous gift from R. DiMarchi, University of Indiana.

Mouse islet isolation. Primary mouse islets were isolated as previously described[45]. Briefly, the pancreas was inflated via the pancreatic duct with collagenase type V (0.8 mg per ml), excised and digested for 10–15 min. The digest was washed with cold RPMI (2 mM L-glutamine, 10 mM glucose, 0.25% BSA, 100 U/ml penicillin, and 100 μg/ml streptomycin), and the islets were separated using a Histopaque gradient. Individual islets were handpicked and either immersed in TRI Reagent for subsequent mRNA isolation or allowed to recover overnight in RPMI with 10% FBS for experiments *ex vivo*.

Primary mouse islet insulin secretion. After overnight incubation, 75–80 medium-sized islets were handpicked into 0.275 ml chambers containing KRB buffer (135 mM NaCl, 3.6 mM KCl, 1.5 mM $CaCl_2$, 0.5 mM NaH_2PO_4, 0.5 mM $MgSO_4$, 5 mM Hepes, 5 mM $NaCO_3$, 0.1% BSA pH 7.5). Islets were perifused for 1 h in KRB with 2.7 mM glucose at a flow rate of 200 μl per min using the Biorep Perifusion system. After this equilibration period, islets were perifused at 8 min intervals in experimental media (KRB plus various conditions), then collected and lysed in acid ethanol for total insulin measurements. Insulin concentrations were determined by radioimmunoassay (Millipore), and insulin secretion was expressed as a percent of total insulin.

Islet hGH release. Isolated islets were incubated in batches of 100 at 37 °C in HEPES Krebs buffer containing 20 mM glucose, as previously described[7]. After 1 h, the buffer was removed and assayed for hGH release using a hGH ELISA (Invitrogen).

Glucose- and insulin-tolerance tests. Oral and intraperitoneal glucose-tolerance tests (GTTs) were performed in mice fasted for 5 h (0700–1200) using a glucose dose of 1.5 g per kg. During IPGTT, mice were i.p. injected with either GIP (4 nmol per kg), Ex4 (0.3 nmol per kg), or saline (veh), 10 min before glucose administration. For tests using a DPP4 inhibitor, sitagliptin (Merck, 40 μg per mouse) was given orally 30 min before glucose. For both OGTT and IPGTT, blood was collected at 0, 10 and 30 min in capillary tubes coated with 10% (vol/vol) TED (500,000 IU/ml Trasylol; 1.2 mg/ml EDTA; and 0.1 mM diprotin A) and plasma separated by centrifugation at 4 °C and stored at −80 °C. Insulin-tolerance tests (ITTs) were performed in mice fasted for 5 h (0700–1200) using an insulin dose of 0.7 U/kg (Humalog, Lilly).

Plasma hormone analysis. Insulin (Alpco Diagnostics) and total GIP (Linco) levels were analyzed by ELISA. Total GLP-1 levels were measured by immunoassay (Mesoscale).

Insulin supplementation. 8-week-old mice had a single insulin pellet (7 or 14 mg, LinBit) inserted into the intrascapular region under isoflurane anesthesia by following the manufacturer's protocol.

Apoptosis *in vivo*. Mice were treated with streptozotocin (Sigma, 50 mg per kg) for 5 consecutive days at 0800. Twenty-four hours after the final treatment, mice were euthanized and the pancreas was excised and immediately immersed in 10% formalin. All histological analysis was performed in a blinded fashion.

Real time quantitative PCR. First-strand cDNA was synthesized from total RNA using the SuperScript III synthesis system (Invitrogen). Real-time PCR was carried out with the ABI Prism 7900 Sequence Detection System using TaqMan Gene Expression Assays (Applied Biosystems). Relative mRNA transcript levels were quantified with the $2^{-\Delta Ct}$ method. PCR primers are shown in **Supplementary Table 1**.

Qualitative PCR. Amplification of mouse *Gipr* cDNA was performed using the primer pairs 5′–CTG CTT CTG CTG CTG TGG T–3′ (forward primer) and 5′–CAC ATG CAG CAT CCC AGA–3′ (reverse primer). PCR was carried out using 35 cycles at an annealing temperature of 50 °C to generate a 1.5 kb product. Amplification of the mouse *Tcf7* isoforms was performed using the common reverse primer 5′–CTA GAG CAC TGT CAT CGG–3′and two different 5′ (forward) primers targeting alternative start codons (1.3 kb product – ATG CCG CAG CTG GAC TCG; 0.9 kb product – ATG TAC AAA GAG ACT GTC TAC T). PCR was carried out using 35 cycles at an annealing temperature of 56 °C.

Western blot analysis. Thirty μg of total protein was separated by SDS-PAGE, transferred to nitrocellulose membranes and blocked in 5% milk in PBS-T for 1 h before incubation in primary antibody overnight at 4 °C. Immunoblots were visualized with the enhanced chemiluminescence Western blot detection kit (PerkinElmer) and quantified with Carestream Molecular Imaging Software (Kodak). Primary antibodies are shown in **Supplementary Table 2**.

Human islet isolation. Primary human islets were isolated as previously described[6] at the Alberta Diabetes Institute Islet Core (http://www.bcell.org/isletcore.html) and the Clinical Islet Isolation Facility at the University of Alberta and cultured in low glucose (5.5 mM) DMEM with L-glutamine, 110 mg per L sodium pyruvate, 10% FBS and 100 U/ml penicillin/streptomycin. We studied islets from 15 non-diabetic, donors (age: 57 ± 11 years; HbA1c: 5.7 ± 1.4 BMI range 19–39) and 4 T2D donors (age: 63 ± 5 years; HbA1c: 6.6 ± 0.9; BMI range- 29–37).

Capacitance measurement. Islets were dispersed in calcium-free dissociation buffer in 35 mm dishes and incubated overnight in RPMI containing 11mM (mouse) or DMEM containing 5.5 mM (human) glucose. GIP (10 nM), Ex4 (1 nM) or vehicle (H_2O) was added to each dish 1 h before patch clamping, using the standard whole-cell technique with the sine + DC lock-in function of an EPC10 amplifier and Patchmaster software (HEKA Electronics). Experiments were performed as described previously[7] at 32–35 °C using an extracellular bath solution (118 mM NaCl, 20 mM TEA, 5.6 mM KCl, 1.2 mM $MgCl_2$, 2.6 mM $CaCl_2$, 5 mM glucose, 5 mM Hepes, pH – 7.4) and pipette solution (125 mM CsGlutamate, 10 mM CsCl, 10 mM NaCl, 1 mM $MgCl_2$, 0.05 mM EGTA, 5 mM Hepes, 3 mM MgATP, 0.1 mM cAMP, pH – 7.15). Capacitance responses to a train of 10 depolarizations from −70 to 0 mV at 1 Hz were normalized to initial cell size and expressed as femtofarad per picofarad (fF/pF). β cells were identified using positive insulin immunostaining.

RNA-seq. Total RNA from isolated islets was extracted using TRI Reagent. The yield and quality of total RNA was assessed using Nanodrop (Thermo Fisher) and BioAnalyzer (Agilent), respectively. Ribosomal RNA was removed using a bead-based hybridization kit (RiboZero, Epicentre) and cDNA libraries were prepared using the Illumina TruSeq RNA sample preparation kit. The quality and concentration of libraries were assessed using BioAnalyzer and qPCR, respectively. The libraries were loaded as two indexed samples per lane on an

doi:10.1038/nm.3997

Illumina HiSeq 2000. Raw sequenced reads were obtained in fastq format, and mapped onto the mouse genome (mm9) using Tophate1.4.1, and then analyzed using a custom R-based pipeline to calculate gene-expression profiles using ENSEMBL annotation for coding genes. The number of reads mapped onto the gene was counted regardless of transcription isoform and normalized to total mapped reads to obtain transcript union Read Per Million total reads (truRPMs). The data have been deposited in NCBI's Gene Expression Omnibus and are accessible through GEO Series accession number GSE65361.

Cell-line culture. INS1823/32 cells were a generous gift from C. Newgard, Duke University. Cells were grown in RPMI (10% FBS, 1% P/S). For GIP experiments, cells were starved in RPMI (1% FBS, 1% P/S) for 3 h. MIN6 cells (from ATCC) were grown in DMEM (20% FBS, 1% P/S). siRNA knockdown experiments were performed by following the manufacturer's instructions (Origene). All cell lines were previously tested for mycoplasma contamination.

Apoptosis assays. *MIN6 beta cells.* After 24 h exposure to thapsigargin (5 uM, Sigma) in culture media (DMEM, 20% FBS, 1% P/S), apoptosis was analyzed using a MitoPT assay (ImmunoChemistry Technologies) by following the kit's instructions. Briefly, cells were exposed to 100 nM MitoPT for 10 min, washed 1 × with PBS and then detached from the plate with trypsin. An aliquot of cells was visualized on a microscope slide. Total cell number was counted using bright field and tetramethylrhodamine methyl ester (TMRM) uptake was visualized with a 545 nM filter. Apoptotic cells were calculated as (total cells – TMRM positive cells)/Total cells × 100%.

Mouse islets. Dispersed islets were transduced with Ad-*GFP* or Ad-*Tcf7-GFP* at an MOI of 10 to achieve a >90% induction rate. After transduction, cells were exposed to control or thapsigargin (100 uM) for 72 h. Apoptosis was assessed using a MitoPT assay.

Human islets. Dispersed human cells were transfected with human si*TCF7* or siScram control duplexes (OriGene, Rockville, MD) and an Alexa488 labeled negative control siRNA (Qiagen, Toronto, ON), using Dharmafect (Thermo Scientific, Ottawa, ON, Canada). 24 h post-transfection culture medium was changed to fresh medium containing glucose and/or human recombinant IL1-β (Sigma, Oakville, ON, Canada), as indicated. Cell-death assays were performed on dispersed human islet cells by use of the *In situ* Cell Death Detection Kit TMR Red (Roche, Mannheim, Germany), using TUNEL technology, according to the manufacturer's directions. Images were obtained using a Zeiss AxioObserver Z1 with a Zeiss-Colibri light source at 488 nm and 594 nm, a × 40/1.3 NA lens, and an AxioCam HRm camera. Images were acquired in Axiovision 4.8 software (Carl Zeiss MicroImaging, Göttingen, Germany) and analyzed using ImageJ software (National Institutes of Health). Cell death was determined as ((#TUNEL+/Alexa488+) / (#Alexa488+)) and expressed as a fold increase over control, unstimulated conditions (5.5mM glucose, scrambled siRNA).

Statistical analysis. All values are presented as mean ± s.e.m. Statistical analysis was performed using GraphPad Prism 5.0. The appropriate *t*-test, one-way analysis of variance (ANOVA), or two-way ANOVA was completed using $P < 0.05$ to signify significant differences. Bonferroni post-hoc analysis was performed where appropriate. All data was assessed to ensure normal distribution and equal variance between groups, using GraphPad Prism 5.0. Prior to the experiment, it was determined that individual data points would be excluded if their value was greater than 2 × SD from the mean, in an experiment with a sample size greater than seven.

41. Wicksteed, B. *et al.* Conditional gene targeting in mouse pancreatic ss-cells: analysis of ectopic Cre transgene expression in the brain. *Diabetes* **59**, 3090–3098 (2010).
42. Scrocchi, L.A. *et al.* Glucose intolerance but normal satiety in mice with a null mutation in the glucagon-like peptide receptor gene. *Nat. Med.* **2**, 1254–1258 (1996).
43. Verbeek, S. *et al.* An HMG-box-containing T-cell factor required for thymocyte differentiation. *Nature* **374**, 70–74 (1995).
44. Patterson, J.T. *et al.* A novel human-based receptor antagonist of sustained action reveals body weight control by endogenous GLP-1. *ACS Chem. Biol.* **6**, 135–145 (2011).
45. Lamont, B.J. *et al.* Pancreatic GLP-1 receptor activation is sufficient for incretin control of glucose metabolism in mice. *J. Clin. Invest.* **122**, 388–402 (2012).

Journal: Nature Medicine

Article Title:	**TCF1 links GIPR signaling to control of β cell function and survival**
Corresponding Author:	Daniel J. Drucker, drucker@lunenfeld.ca

Supplementary Item & Number	Title or Caption
Supplementary Figure 1	Generation of *Gipr*$^{-/-\beta Cell}$ mice.
Supplementary Figure 2	Phenotype of *Gipr*$^{-/-\beta Cell}$ mice.
Supplementary Figure 3	Characterization of *Gipr*$^{-/-\beta Cell}$ islets.
Supplementary Figure 4	Diabetic *db/db* mice fail to lower glucose in response to exogenous GIP
Supplementary Figure 5	Phenotype of *Tcf7*$^{-/-}$ mice
Supplementary Figure 6	Glycemic and insulin response to incretin receptor agonists and DPP4 inhibition in *Tcf7*$^{-/-}$ mice.
Supplementary Figure 7	Representative images of cells following adenoviral transduction and apoptotic index following treatment with or without thapsigargin.
Supplementary Figure 8	Representative image of apoptotic index and *Tcf7* knockdown in MIN6 β cells
Supplementary Table 1	List of real time primers
Supplementary Table 2	List of antibodies
Supplementary Methods	

Supplementary Figure 1

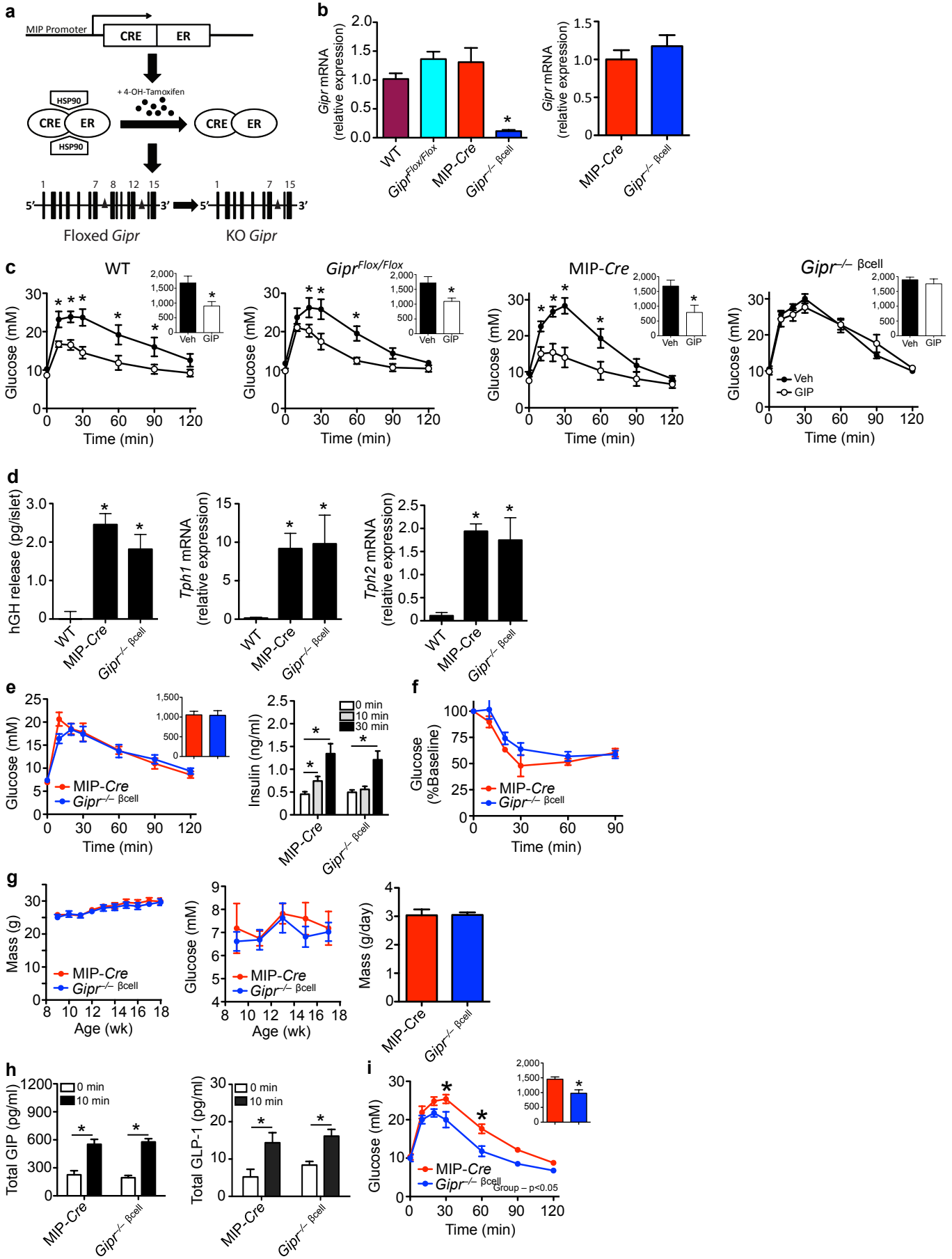

Supplementary Figure 2

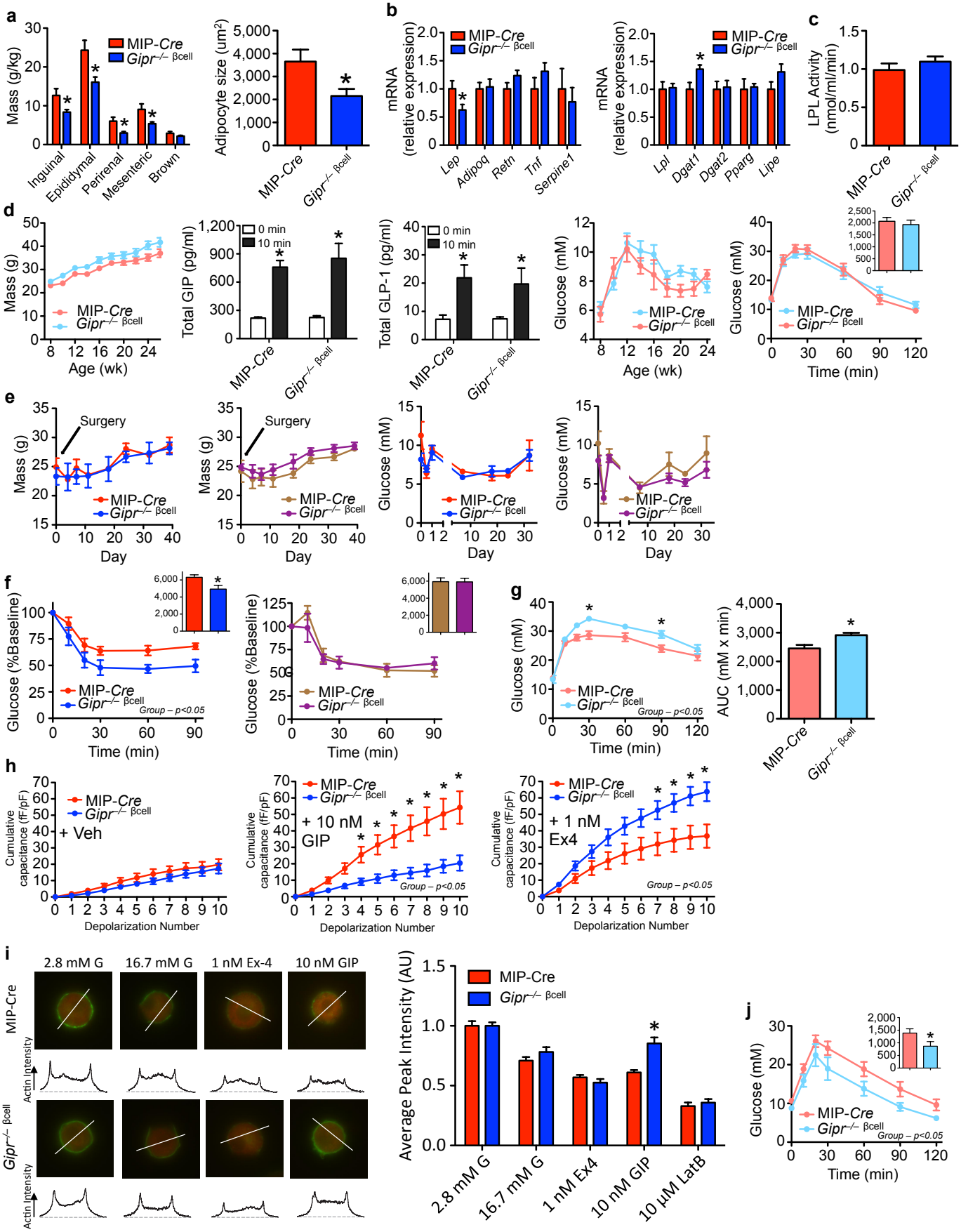

Nature Medicine: doi:10.1038/nm.3997

Supplementary Figure 3

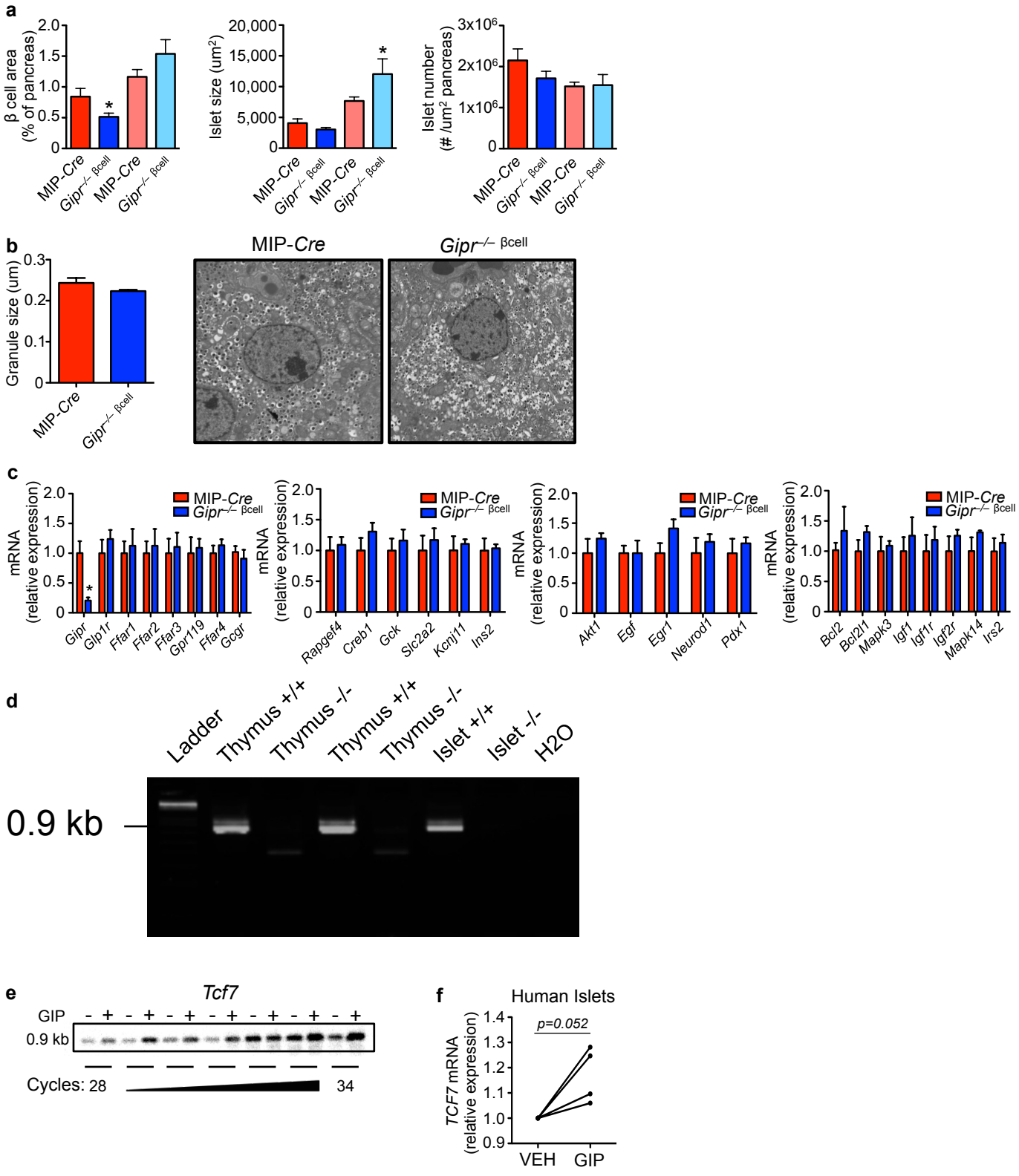

Supplementary Figure 4

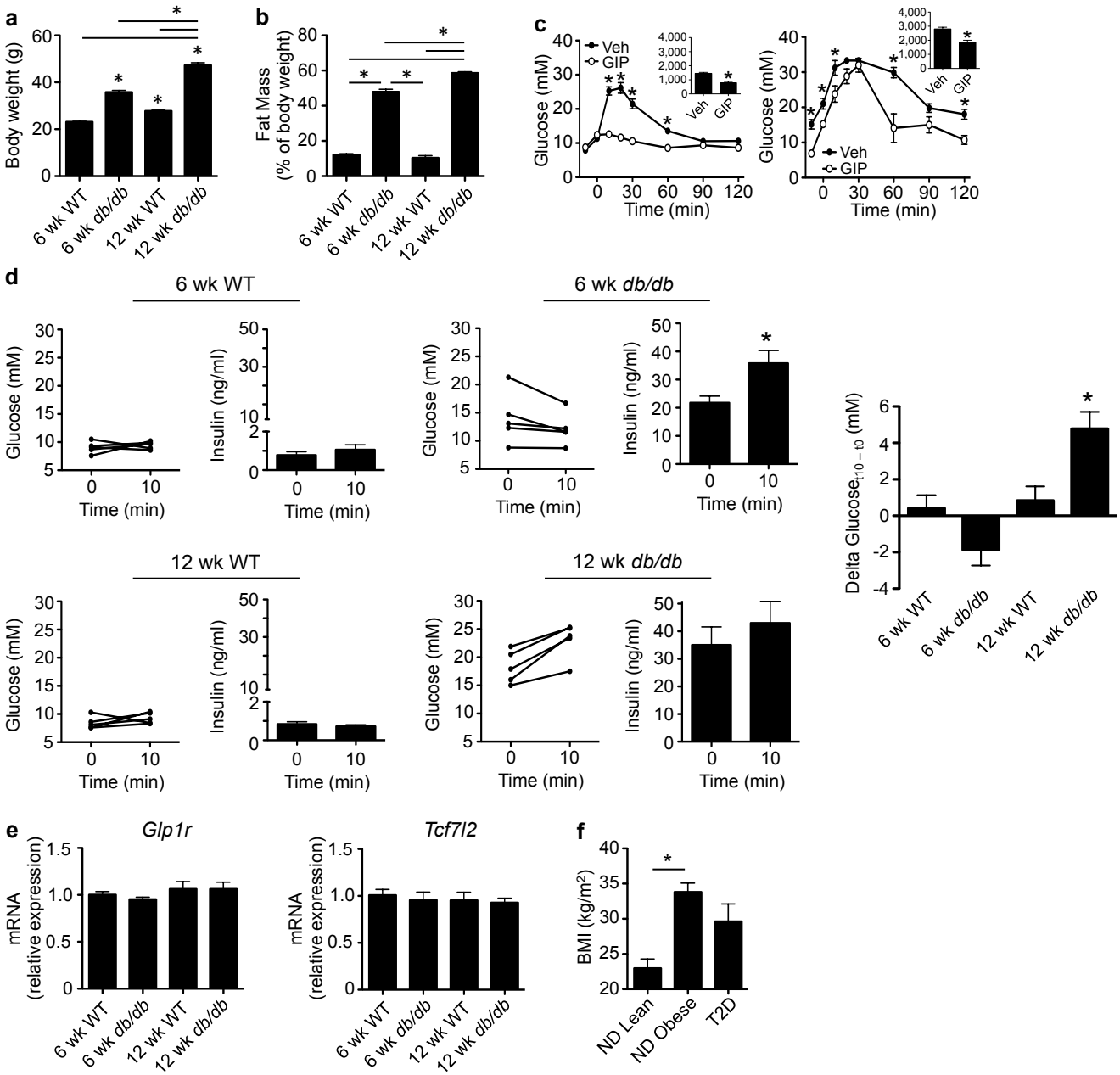

Supplementary Figure 5

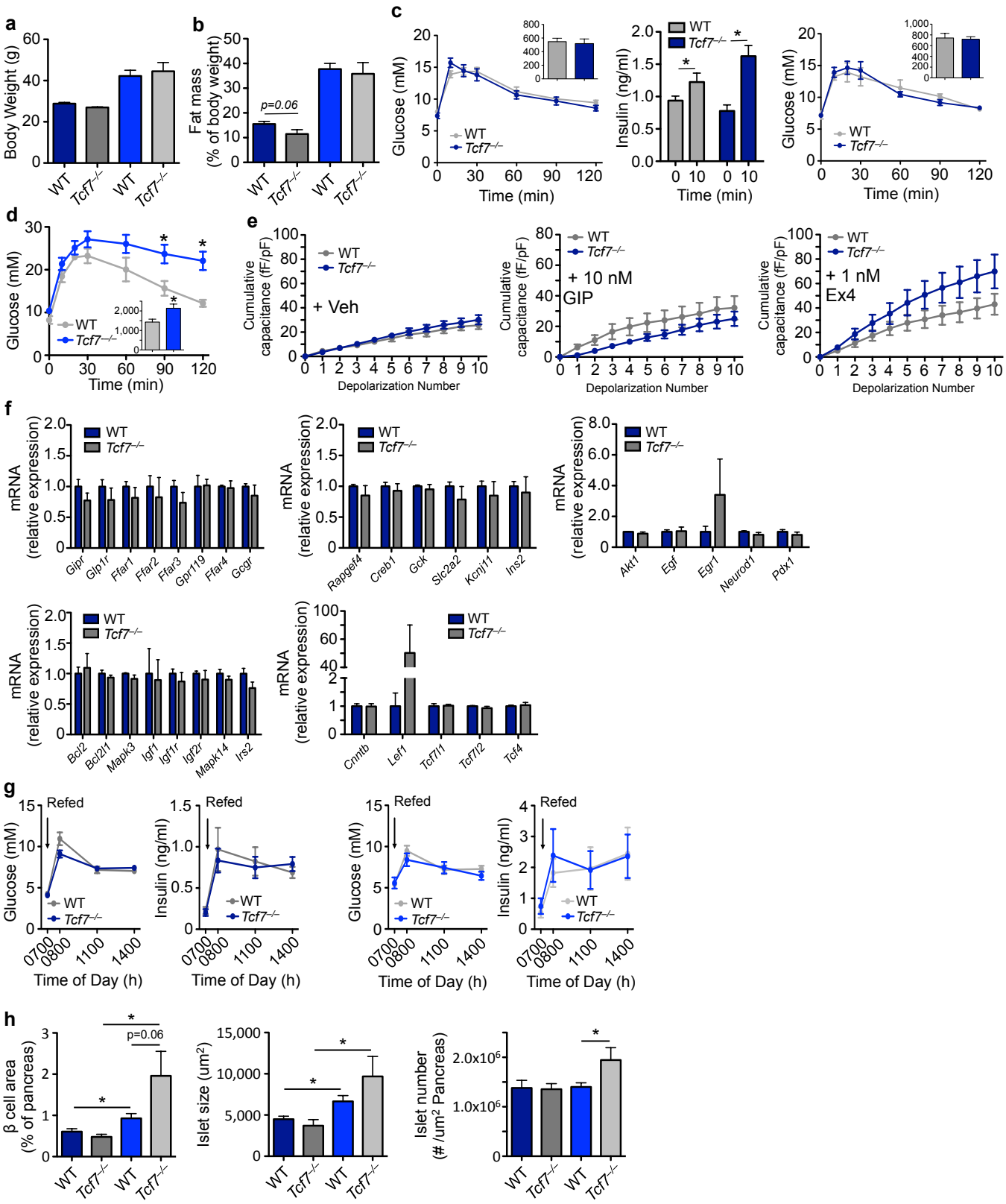

Supplementary Figure 6

Low-Fat Diet:

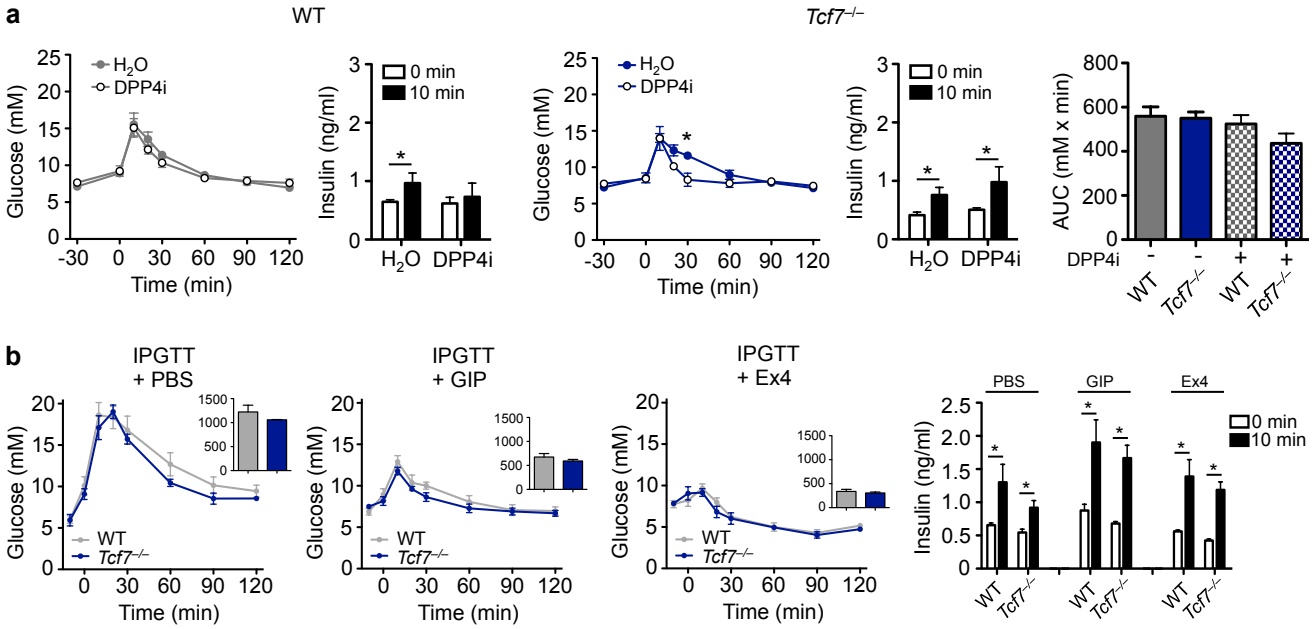

High-Fat Diet:

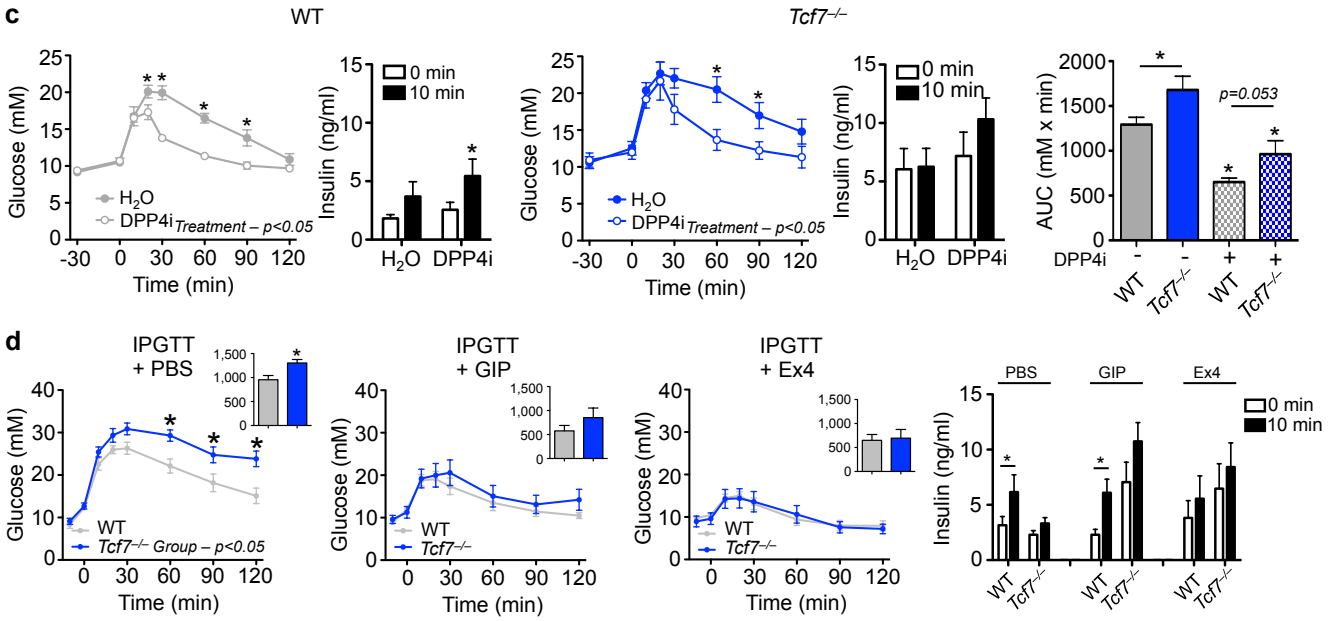

Supplementary Figure 7

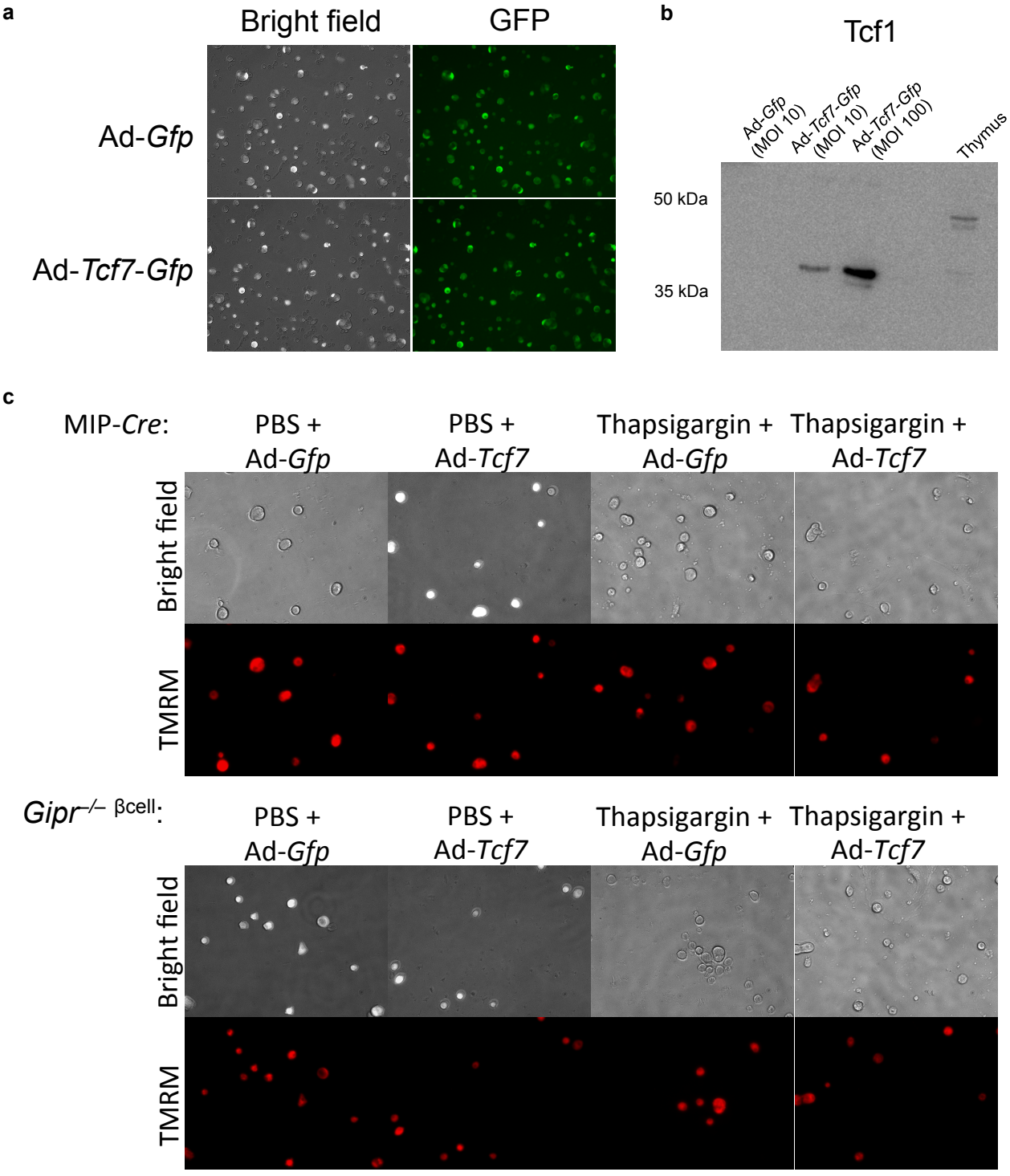

Supplementary Figure 8

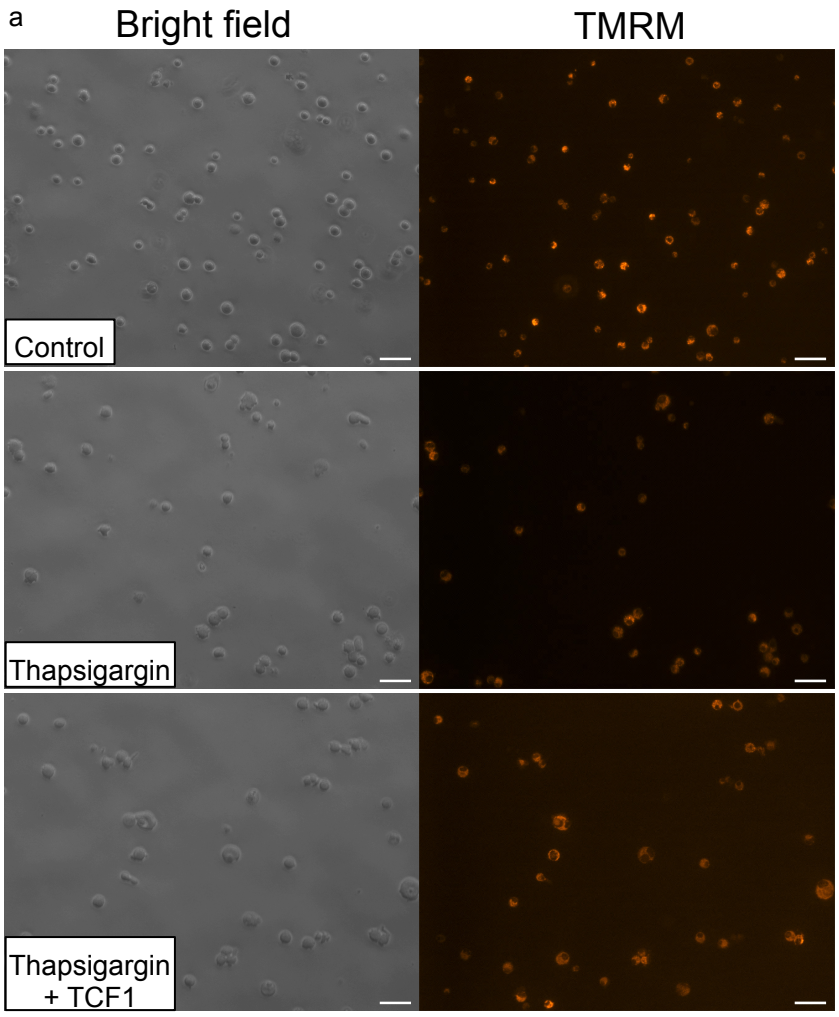

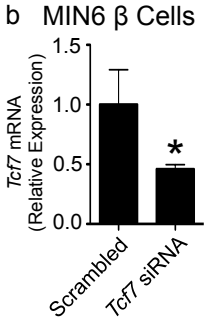

Supplementary Table 1. List of Real-Time Primers

	Gene	ABI Catalog #	Amplicon Length
Mouse	*Adipoq*	Mm00456425_m1	74
	Akt1	Mm01331626_m1	69
	Bcl2	Mm00477631_m1	85
	Bcl2l1	Mm00437783_m1	65
	Birc2	Mm00431811_m1	90
	Birc3	Mm00431800_m1	61
	Creb1	Mm00501607_m1	106
	Ctnnb1	Mm00483039_m1	77
	Dgat1	Mm00515643_m1	66
	Dgat2	Mm01273905_m1	74
	Egf	Mm00438696_m1	96
	Egr1	Mm00656724_m1	182
	Ffar1	Mm00809442_m1	147
	Ffar2	Mm02620654_s1	147
	Ffar3	Mm02621638_s1	140
	Ffar4	Mm00725193_m1	79
	Gck	Mm00439129_m1	69
	Gipr	Mm01316344_m1	92
	Glp1r	Mm01351008_m1	94
	Gpr119	Mm00731497_s1	63
	Hif1a	Mm00468869_m1	75
	Igf1	Mm00439561_m1	69
	Igf1r	Mm00802831_m1	106
	Igfr2	Mm00439576_m1	64
	Ins2	Mm00731595_gH	99
	Irs2	Mm03038438_m1	63
	Kcnj11	Mm00440050_m1	129
	Lef1	Mm00550265_m1	84
	Lep	Mm004346579_m1	73
	Lipe	Mm00495359_m1	70
	Lpl	Mm00434770_m1	77
	Mapk14	Mm00442497_m1	56
	Mapk3	Mm01973540_g1	98
	Neurod1	Mm01280117_m1	81
	Pdx1	Mm00435565_m1	74
	Pparg	Mm01184322_m1	101
	Ppia	Mm02342430_g1	148
	Pttg1	Mm00479224_m1	72
	Rapgef4	Mm00517216_m1	67
	Retn	Mm00445641_m1	80
	Serpine1	Mm00435860_m1	60
	Slc2a2	Mm00446224_m1	83
	Tcf4	Mm00443210_m1	98
	Tcf7	Mm00493445_m1	91
	Tcf7l1	Mm01188711_m1	78
	Tcf7l2	Mm00501505_m1	85
	Tph1	Mm01202614_m1	103
	Tph2	Mm00557717_m1	82
	Tnf	Mm00443258_m1	81
	Xiap	Mm00776505_m1	144
Rat	*Tcf7*	Rn01463535_m1	68
	Ppia	Rn00690933	149
Human	*TCF7*	Hs00175273_m1	105
	GAPDH	Hs99999905	122

Supplementary Table 2 List of Antibodies

Protein	Company	Catalog #
TCF1	Cell Signaling Technologies	2206
Lamin A/C	Cell Signaling Technologies	2032
phosphoERK	Cell Signaling Technologies	9101
ERK	Cell Signaling Technologies	9102
Cleaved Caspase 3	Cell Signaling Technologies	9661
Caspase 3	Cell Signaling Technologies	9662
HSP90	BD Biosciences	610418

All Cell signaling technologies antibodies are profiled on antibodypedia.

Supplemental Information

TCF1 links GIPR signaling to the control of β cell function and survival

Jonathan E Campbell[1], John R Ussher[1,7], Erin E Mulvihill[1], Jelena Kolic[2,3], Laurie L Baggio[1], Xiemen Cao[1], Yu Liu[1], Benjamin J Lamont[1,7], Tsukasa Morii[1,7], Catherine J Streutker[4], Natalia Tamarina[5], Louis H Philipson[5], Jeffrey L Wrana[1], Patrick E MacDonald[2,3] & Daniel J Drucker[1,6]

Supplemental Figure 1 Generation of *Gipr*$^{-/-\beta Cell}$ mice. **(a)** Schematic illustrating the generation of *Gipr*$^{-/-\beta Cell}$ mice. **(b)** *Gipr* expression in mouse islets (left, n=3, 5, 3, and 5) and epididymal adipose tissue (right, n=7). **(c)** Intraperitoneal glucose tolerance test (IPGTT) in 10-week-old mice fed a LFD (n=8, 4, 7, and 5). **(d)** hGH release (left) from mouse islets in culture, *Tph1* (middle) and *Tph2* (right) expression in mouse islets (n=5, 5, and 6). **(e)** Glycemic (left) and insulin (right) response during an oral glucose tolerance test (OGTT) in 10-week-old mice fed a LFD (n=7). **(f)** Glycemic response during an intraperitonel insulin tolerance test in 8-week-old mice fed a LFD (n=4 and 6). **(g)** Body weight (left), fed glucose values (middle), and average food intake (right) in mice fed a LFD (n=7). **(h)** Total GIP (left) and GLP-1 (right) plasma concentration during an OGTT in mice fed a LFD (n=7). **(i)** IPGTT in 18-week-old mice fed a LFD (n=7). **P*<0.05 vs control, or as indicated. Data are expressed as Mean± SEM. Statistical tests used: t-test – for g (right) and AUC inset (c, e and i); 1-way analysis of variance (ANOVA) – for b and d; 2-way ANOVA - for c, and e-i. LFD – low fat diet, GIP – glucose-dependent insulinotropic polypeptide, GLP-1 – glucagon-like peptide 1.

Supplemental Figure 2 Phenotype of *Gipr*$^{-/-\beta Cell}$ mice. **(a)** Adipose depot weights (left) and epididymal adipocyte size (right) from 20-week-old mice (n=7). **(b)** qPCR analysis of genes important for adipose tissue metabolism (n=7). **(c)** Lipoprotein lipase activity in epididymal adipose depots from 20-week-old mice (n=7). **(d)** (left to right) Body weight (n=9 and 13), plasma total GIP concentrations (n=9), plasma total GLP-1 concentrations (n=9), fed glycemia (n=9 and 13), and intraperitoneal glucose tolerance test (IPGTT) (n=9 and 13) in mice fed a HFD. **(e)** Body weight (two left panels) and glycemia (two right panels) following sham (blue and red) or insulin pellet (purple and brown) surgery (n=3, 5, 3, and 6; *MIP-Cre* (sham), *Gipr*$^{-/-\beta Cell}$ (sham), *MIP-Cre* (pellet), and *Gipr*$^{-/-\beta Cell}$ (pellet)). **(f)** Glycemic response to insulin tolerance test in 18-week-old mice following sham (left) or insulin pellet (right) surgery (n=3, 5, 3, and 6; *MIP-Cre* (sham), *Gipr*$^{-/-\beta Cell}$ (sham), *MIP-Cre* (pellet), and *Gipr*$^{-/-\beta Cell}$ (pellet)). **(g)** Glycemic response during an oral glucose tolerance test in 16-week-old mice fed a HFD and given a GLP-1R antagonist (n=9). (**h**) Cumulative capacitance in isolated β cells determined by whole cell patch clamping , treated with vehicle (left panel), GIP (middle panel) or exendin-4 (right panel) **(i)** Actin intensity in individual β cells stimulated with low glucose (n=55 and 42, *MIP-Cre* and *Gipr*$^{-/-\beta Cell}$) 16.7 mM glucose (n=48 and 51, *MIP-Cre* and *Gipr*$^{-/-\beta Cell}$), 1 nM Ex4 (n=46 and 44, *MIP-Cre* and *Gipr*$^{-/-\beta Cell}$), 10 nM GIP (n=47 and 44, *MIP-Cre* and *Gipr*$^{-/-\beta Cell}$), or 10 uM latrunculin B (LatB) (n=42 and 32, *MIP-Cre* and *Gipr*$^{-/-\beta Cell}$). **(j)** IPGTT in 16-week-old mice given a GPR119 agonist (n=8 and 13). **P*<0.05 vs control. Data are expressed as Mean± SEM. Statistical tests used: t-test – for a-c and i, and AUC (d, f and

g); 2-way analysis of variance (ANOVA) – for d-g. GIP – glucose-dependent insulinotropic polypeptide, GLP-1 – glucagon-like peptide 1, HFD – high fat diet.

Supplemental Figure 3 Characterization of *Gipr*$^{-/-\beta Cell}$ islets. **(a)** Histological analysis of β cell area (left), islet size (middle), and islet number (right) in samples from mice fed a LFD (red and blue, n=7 and 7) or HFD (pink and light blue, n=9 and 13). **(b)** Electron microscopy showing insulin granular size in pancreata samples from mice fed a LFD (n=7). **(c)** qPCR analysis of RNA from isolated islets from 20-week-old mice fed a LFD (n=7). **(d)** Representative image of *Tcf7* expression in RNA from thymus and islets from 8-week-old mice fed a LFD. **(e)** Representative image of *Tcf7* expression in islets treated with Veh (-) or GIP (+) following sequential PCR cycling (n=3). **(f)** *TCF7* expression in human islets treated with Veh or GIP (n=4). **P*<0.05 vs control. Data are expressed as Mean± SEM. Statistical tests used: t-test – for b, c and f; 2-way analysis of variance (ANOVA) – for a. Veh – vehicle, GIP – glucose-dependent insulinotropic polypeptide. LFD – low fat diet, HFD – high fat diet.

Supplemental Figure 4 Diabetic *db/db* mice fail to lower glucose in response to exogenous GIP. **(a)** Body weight (n=5). **(b)** Body adiposity determined by MRI (n=5). **(c)** Glycemic response during an intraperitoneal glucose tolerance test in 6-week-old WT (left) and *db/db* (right) mice (n=5). **(d)** Glycemic response to exogenous GIP in random fed mice (n=5). **(e)** *Glp1r* (left) and *Tcf7l2* (right) expression in RNA from mouse islets (n=5). **(f)** Body mass index in human subjects (n=5, 5, and 4). **P*<0.05 vs control, or as indicated. Data are expressed as Mean± SEM. Statistical tests used: t-test – for b, c and f; 2-way analysis of variance (ANOVA) – for a. Veh – vehicle, GIP – glucose-dependent insulinotropic polypeptide, ND – non-diabetic, T2D – type 2 diabetic.

Supplemental Figure 5 Phenotype of *Tcf7*$^{-/-}$ mice. **(a)** Body weight in 18-week-old mice fed a LFD (dark blue and dark grey, n=7 and 5) or HFD (light blue and light grey, n=10 and 7). **(b)** Body adiposity determined by MRI in mice fed a LFD (dark blue and dark grey) or HFD (light blue and light grey) (n=7, 5, 10, and 7). **(c)** Glycemic (left) and insulin (middle) response during an oral glucose tolerance test (OGTT) and glycemic (right) response during an intraperitoneal glucose test (IPGTT) in 8-week-old mice on a LFD (n=7 and 8). **(d)** Glycemic response during an IPGTT in 12-week-old mice on a HFD (n=10 and 7). **(e)** Cumulative capacitance in individual β cells stimulated with Veh (left, n=18 and 20), GIP (middle, n=18 and 18), or Ex4 (right, n=15 and 17). **(f)** qPCR analysis of RNA from islets from 18-week-old mice fed a LFD (n=4). **(g)** Glycemic and insulin response during a fasting-refeeding test in 10-week-old mice fed a LFD (two left panels, n=7 and 5) or HFD (two right panels, n=7 and 10). **(h)** Histological analysis of β cell area (left), islet size (middle), and islet number (right) in samples from mice fed a LFD (dark blue and grey, n=7 and 5) or HFD (light blue and light grey, n=10 and 7). **P*<0.05 vs control, or as indicated. Data are expressed as Mean± SEM. Statistical tests used: t-test – for f and AUC inset (c and d); 2-way analysis of variance (ANOVA) – for a-e, g, h. LFD- low fat diet, HFD – high fat diet, Veh – vehicle, GIP – glucose-dependent insulinotropic polypeptide, Ex4 – exendin-4.

Supplemental Figure 6 Glycemic and insulin response to incretin receptor agonists and DPP4 inhibition in *Tcf7*$^{-/-}$ mice. **(a)** Glycemic and insulin response during an oral glucose tolerance test (OGTT) in 12-week-old mice fed a LFD (n=5). **(b)** Glycemic and insulin response during an intraperitoneal glucose tolerance test (IPGTT) in 12-week-old mice fed a LFD (n=7 and 5, WT and *Tcf7*$^{-/-}$). **(c)** Glycemic and insulin response during an OGTT in 12-week-old mice fed a HFD (n=9). **(b)** Glycemic and insulin response during and intraperitoneal glucose tolerance test (IPGTT) in 12-week-old mice fed a HFD (n=10 and 8 WT and *Tcf7*$^{-/-}$). **P*<0.05 vs control, or as indicated. Data are expressed as Mean± SEM. Statistical test used: 2-way analysis of variance (ANOVA). LFD- low fat diet, HFD – high fat diet, DPP4i – dipeptidyl peptidase 4 inhibitor, Veh – vehicle, GIP – glucose-dependent insulinotropic polypeptide, Ex4 – exendin-4.

Supplemental Figure 7 Representative images of adenoviral transduction and apoptotic index. **(a)** Representative image of bright field and GFP (495 nm) in mouse β cells. **(b)** Tcf1 protein expression in baby hamster kidney (BHK) fibroblast cells and mouse thymus. **(c)** Representative images of bright field and TMRM (545 nm) in mouse β cells.

Supplemental Figure 8 Representative image of apoptotic index and *Tcf7* knockdown in MIN6 β cells. **(a)** Representative images of bright field and TMRM (545 nm) in MIN6 β cells. **(b)** *Tcf7* expression in MIN6 β cells (n=6). **P*<0.05 vs control, or as indicated. Data are expressed as Mean± SEM. Statistical test used: t-test – for b.

Online Methods

Animals.

Male mice were used for all mouse studies and were maintained under a 12 h light/12 h dark cycle at constant temperature (23 °C) with free access to food and water. All animal studies were approved by Mt. Sinai Hospital (Toronto) and the Toronto Centre for Phenogenomics animal-care committee. Animals were fed either a low-fat diet (10% kcal from fat; Research Diets, D12450B) or high-fat diet (45% kcal from fat; Research Diets, D12451). To generate $Gipr^{-/-\beta Cell}$ mice, MIPcreER transgenic mice (on a C57BL/6J background) expressing tamoxifen-inducible Cre driven by the mouse insulin promoter were bred with floxed *Gipr* mice ($Gipr^{Flox/Flox}$), backcrossed 8 times to C57BL/6J background)[41]. Cre-induced inactivation of the *Gipr* gene was carried out via 5 consecutive daily intraperitoneal (*i.p.*) injections of tamoxifen (40 mg per kg) in 6-week-old mice. $Glp1r^{-/-}$ and $Tcf7^{-/-}$ mice (both on C57BL/6J backgrounds) have been previously described[42,43]. $Tcf7^{-/-}$ mice were generously provided by H. Clevers, *db/db* mice were purchased from Jackson laboratories (#000697). For all animal experiments, the sample size required to achieve adequate power was estimated on the basis of pilot work or previous experiments. When appropriate, animals were randomly allocated to individual experimental groups.

Peptides and reagents.

Peptides were reconstituted in phosphate-buffered saline (PBS), aliquoted and stored at –80 °C. [D-Ala^2]GIP (GIP) was from Chi Scientific, Ex4 (exendin-4) was from California Peptide Research Inc. Plasmid constructs (*Tcf7* and *Pttg1*) and siRNA (*Gipr*, *Glp1r*, *Tcf7*, *TCF7*) were from Origene. The GLP-1R antagonist (JANT-4)[44] was a generous gift from R. DiMarchi, University of Indiana.

Mouse islet isolation.

Primary mouse islets were isolated as previously described[45]. Briefly, the pancreas was inflated via the pancreatic duct with collagenase type V (0.8 mg per ml), excised and digested for 10–15 min. The digest was washed with cold RPMI (2 mM L-glutamine, 10 mM glucose, 0.25% BSA, 100 U/ml penicillin, and 100 µg/ml streptomycin), and the islets were separated using a Histopaque gradient. Individual islets were handpicked and either immersed in TRI Reagent for subsequent mRNA isolation or allowed to recover overnight in RPMI with 10% FBS for experiments *ex vivo*.

Primary mouse islet insulin secretion.

After overnight incubation, 75–80 medium-sized islets were handpicked into 0.275 ml chambers containing KRB buffer (135 mM NaCl, 3.6 mM KCl, 1.5 mM $CaCl_2$, 0.5 mM NaH_2PO_4, 0.5 mM $MgSO_4$, 5 mM Hepes, 5 mM $NaCO_3$, 0.1% BSA pH 7.5). Islets were perifused for 1 h in KRB with 2.7 mM glucose at a flow rate of 200 µl per min using the Biorep Perifusion system. After this equilibration period, islets were perifused at 8 min intervals in experimental media (KRB plus various conditions), then collected and lysed in acid ethanol for total insulin measurements. Insulin concentrations were determined by radioimmunoassay (Millipore), and insulin secretion was expressed as a percent of total insulin.

Islet hGH release.

Isolated islets were incubated in batches of 100 at 37 °C in HEPES Krebs buffer containing 20 mM glucose, as previously described[7]. After 1 h, the buffer was removed and assayed for hGH release using a hGH ELISA (Invitrogen).

Glucose- and insulin-tolerance tests.

Oral and intraperitoneal glucose-tolerance tests (GTTs) were performed in mice fasted for 5 h (0700–1200) using a glucose dose of 1.5 g per kg. During IPGTT, mice were i.p. injected with either GIP (4 nmol per kg), Ex4 (0.3 nmol per kg), or saline (veh), 10 min before glucose administration. For tests using a DPP4 inhibitor, sitagliptin (Merck, 40 μg per mouse) was given orally 30 min before glucose. For both OGTT and IPGTT, blood was collected at 0, 10 and 30 min in capillary tubes coated with 10% (vol/vol) TED (500,000 IU/ml Trasylol; 1.2 mg/ml EDTA; and 0.1 mM diprotin A) and plasma separated by centrifugation at 4 °C and stored at –80 °C. Insulin-tolerance tests (ITTs) were performed in mice fasted for 5 h (0700–1200) using an insulin dose of 0.7 U/kg (Humalog, Lilly).

Plasma hormone analysis.

Insulin (Alpco Diagnostics) and total GIP (Linco) levels were analyzed by ELISA. Total GLP-1 levels were measured by immunoassay (Mesoscale).

Insulin supplementation.

8-week-old mice had a single insulin pellet (7 or 14 mg, LinBit) inserted into the intrascapular region under isoflurane anesthesia by following the manufacturer's protocol.

Apoptosis *in vivo*.

Mice were treated with streptozotocin (Sigma, 50 mg per kg) for 5 consecutive days at 0800. Twenty-four hours after the final treatment, mice were euthanized and the pancreas was excised and immediately immersed in 10% formalin. All histological analysis was performed in a blinded fashion.

Real time quantitative PCR.

First-strand cDNA was synthesized from total RNA using the SuperScript III synthesis system (Invitrogen). Real-time PCR was carried out with the ABI Prism 7900 Sequence Detection System using TaqMan Gene Expression Assays (Applied Biosystems). Relative mRNA transcript levels were quantified with the $2^{-\Delta Ct}$ method. PCR primers are shown in **Supplementary Table 1**.

Qualitative PCR.

Amplification of mouse *Gipr* cDNA was performed using the primer pairs 5′–CTG CTT CTG CTG CTG TGG T–3′ (forward primer) and 5′–CAC ATG CAG CAT CCC AGA–3′ (reverse primer). PCR was carried out using 35 cycles at an annealing temperature of 50 °C to generate a 1.5 kb product. Amplification of the mouse *Tcf7* isoforms was performed using the common reverse primer 5′–CTA GAG CAC TGT CAT CGG–3′and

two different 5′ (forward) primers targeting alternative start codons (1.3 kb product – ATG CCG CAG CTG GAC TCG; 0.9 kb product – ATG TAC AAA GAG ACT GTC TAC T). PCR was carried out using 35 cycles at an annealing temperature of 56 °C.

Western blot analysis.

Thirty μg of total protein was separated by SDS-PAGE, transferred to nitrocellulose membranes and blocked in 5% milk in PBS-T for 1 h before incubation in primary antibody overnight at 4 °C. Immunoblots were visualized with the enhanced chemiluminescence Western blot detection kit (Perkin Elmer) and quantified with Carestream Molecular Imaging Software (Kodak). Primary antibodies are shown in **Supplementary Table 2**.

Human islet isolation.

Primary human islets were isolated as previously described[6] at the Alberta Diabetes Institute Islet Core (www.bcell.org/isletcore.html) and the Clinical Islet Isolation Facility at the University of Alberta and cultured in low glucose (5.5 mM) DMEM with L-glutamine, 110 mg per L sodium pyruvate, 10% FBS and 100 U/ml penicillin/streptomycin. We studied islets from 15 non-diabetic, lean donors (age: 57 ± 11 years; HbA1c: 5.7 ± 1.4 BMI range 19–39) and 4 T2D donors (age: 63 ± 5 years; HbA1c: 6.6 ± 0.9; BMI range- 29–37).

Capacitance measurement.

Islets were dispersed in calcium-free dissociation buffer in 35 mm dishes and incubated overnight in RPMI containing 11mM (mouse) or 5.5 mM (human) glucose. GIP (10 nM), Ex4 (1 nM) or vehicle (H_2O) was added to each dish 1 h before patch clamping, using the standard whole-cell technique with the sine + DC locking function of an EPC10 amplifier and Patchmaster software (HEKA Electronics). Experiments were performed as described previously[7] at 32–35 °C using an extracellular bath solution (118 mM NaCl, 20 mM TEA, 5.6 mM KCl, 1.2 mM $MgCl_2$, 2.6 mM $CaCl_2$, 5 mM glucose, 5 mM Hepes, pH – 7.4) and pipette solution (125 mM CsGlutamate, 10 mM CsCl, 10 mM NaCl, 1 mM $MgCl_2$, 0.05 mM EGTA, 5 mM Hepes, 3 mM MgATP, 0.1 mM cAMP, pH – 7.15). Capacitance responses to a train of 10 depolarizations from –70 to 0 mV at 1 Hz were normalized to initial cell size and expressed as femtofarad per picofarad (fF/pF). β cells were identified using positive insulin immunostaining.

RNA-seq.

Total RNA from isolated islets was extracted using TRI Reagent. The yield and quality of total RNA was assessed using Nanodrop (Thermo Fisher) and BioAnalyzer (Agilent), respectively. Ribosomal RNA was removed using a bead-based hybridization kit (RiboZero, Epicentre) and cDNA libraries were prepared using the Illumina TruSeq RNA sample preparation kit. The quality and concentration of libraries were assessed using BioAnalyzer and qPCR, respectively. The libraries were loaded as two indexed samples per lane on an Illumina HiSeq 2000. Raw sequenced reads were obtained in fastq format, and mapped onto the mouse genome (mm9) using Tophate1.4.1, and then analyzed using a custom R-based pipeline to calculate gene-expression profiles using ENSEMBL annotation for coding genes. The number of reads mapped onto the gene was counted

regardless of transcription isoform and normalized to total mapped reads to obtain transcript union Read Per Million total reads (truRPMs). The data have been deposited in NCBI's Gene Expression Omnibus and are accessible through GEO Series accession number GSE65361.

Cell-line culture.

INS1823/32 cells were a generous gift from C. Newgard, Duke University. Cells were grown in RPMI (10% FBS, 1% P/S). For GIP experiments, cells were starved in RPMI (1% FBS, 1% P/S) for 3 h. MIN6 cells (from ATCC) were grown in DMEM (20% FBS, 1% P/S). siRNA knockdown experiments were performed by following the manufacturer's instructions (Origene). All cell lines were previously tested for mycoplasma contamination.

Apoptosis assays.

MIN6 beta cells. After 24 h exposure to thapsigargin (5 uM, Sigma) in culture media (DMEM, 20% FBS, 1% P/S), apoptosis was analyzed using a MitoPT assay (ImmunoChemistry Technologies) by following the kit's instructions. Briefly, cells were exposed to 100 nM MitoPT for 10 min, washed 1 × with PBS and then detached from the plate with trypsin. An aliquot of cells was visualized on a microscope slide. Total cell number was counted using bright field and tetramethylrhodamine methyl ester (TMRM) uptake was visualized with a 545 nM filter. Apoptotic cells were calculated as (total cells – TMRM positive cells)/Total cells × 100%.

Mouse islets. Dispersed islets were transduced with Ad-*GFP* or Ad-*Tcf7-GFP* at an MOI of 10 to achieve a >90% induction rate. After transduction, cells were exposed to control or thapsigargin (100 uM) for 72 h. Apoptosis was assessed using a MitoPT assay.

Human islets. Dispersed human cells were transfected with human si*TCF7* or siScram control duplexes (OriGene, Rockville, MD) and an Alexa488 labeled negative control siRNA (Qiagen, Toronto, ON), using Dharmafect (Thermo Scientific, Ottawa, ON, Canada). 24 h post-transfection culture medium was changed to fresh medium containing glucose and/or human recombinant IL1-β (Sigma, Oakville, ON, Canada), as indicated. Cell-death assays were performed on dispersed human islet cells by use of the *In situ* Cell Death Detection Kit TMR Red (Roche, Mannheim, Germany), using TUNEL technology, according to the manufacturer's directions. Images were obtained using a Zeiss AxioObserver Z1 with a Zeiss-Colibri light source at 488 nm and 594 nm, a × 40/1.3 NA lens, and an AxioCam HRm camera. Images were acquired in Axiovision 4.8 software (Carl Zeiss MicroImaging, Göttingen, Germany) and analyzed using ImageJ software (National Institutes of Health). Cell death was determined as ((#TUNEL+/Alexa488+) / (#Alexa488+)) and expressed as a fold increase over control, unstimulated conditions (5.5mM glucose, scrambled siRNA).

Statistical analysis.

All values are presented as mean ± s.e.m. Statistical analysis was performed using GraphPad Prism 5.0. The appropriate *t*-test, one-way analysis of variance (ANOVA), or two-way ANOVA was completed using $P < 0.05$ to signify significant differences. Bonferroni post-hoc analysis was performed where appropriate. All data was assessed to

ensure normal distribution and equal variance between groups, using GraphPad Prism 5.0. Prior to the experiment, it was determined that individual data points would be excluded if their value was greater than 2 × SD from the mean, in an experiment with a sample size greater than seven.

41. Wicksteed, B. *et al.* Conditional gene targeting in mouse pancreatic ss-cells: analysis of ectopic Cre transgene expression in the brain. *Diabetes* **59**, 3090–3098 (2010).

42. Scrocchi, L.A. *et al.* Glucose intolerance but normal satiety in mice with a null mutation in the glucagon-like peptide receptor gene. *Nat. Med.* **2**, 1254–1258 (1996).

43. Verbeek, S. *et al.* An HMG-box-containing T-cell factor required for thymocyte differentiation. *Nature* **374**, 70–74 (1995).

44. Patterson, J.T. *et al.* A novel human-based receptor antagonist of sustained action reveals body weight control by endogenous GLP-1. *ACS Chem. Biol.* **6**, 135–145 (2011).

45. Lamont, B.J. *et al.* Pancreatic GLP-1 receptor activation is sufficient for incretin control of glucose metabolism in mice. *J. Clin. Invest.* **122**, 388–402 (2012).